View Article Online
View Journal

# Nanoscale Horizons

The home for rapid reports of exceptional significance in nanoscience and nanotechnology

## Accepted Manuscript

This article can be cited before page numbers have been issued, to do this please use: X. Li, S. Wang, M. Zheng, Z. Ma, Y. Chen, L. Deng, W. xu, F. Guang, S. Khademolqorani, S. N. Banitaba and A. I. Osman, *Nanoscale Horiz.*, 2024, DOI: 10.1039/D4NH00209A.

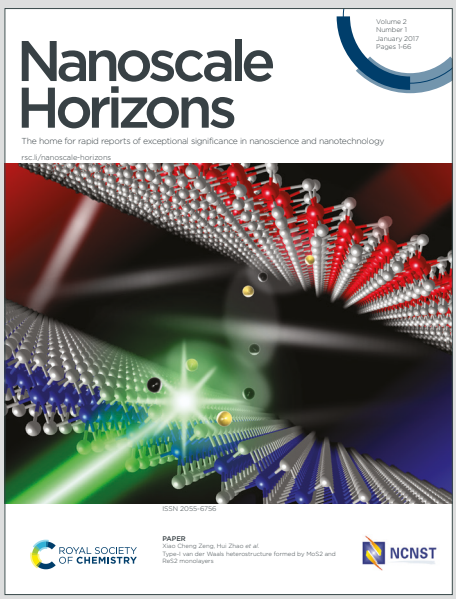

## Data Availability Statement

View Article Online
DOI: 10.1039/D4NH00209A

No new data were generated or analyzed in this study. All data supporting the findings of this study are available from the referenced articles within the review.



View Article Online
DOI: 10.1039/D4NH00209A

# Synergistic Integration of MXene Nanostructures into Electrospun Fibers for Advanced Biomedical Engineering Applications

Xiaobo Li[1], Shan Wang[1], Minyan Zheng[1], Zhanying Ma[1], Yan Chen[1], Lingjuan Deng[1], Weixia Xu[1], Guang Fan[1]*, Sanaz Khademolqorani[2], Seyedeh Nooshin Banitaba[2], Ahmed I. Osman[3]*

[1] School of Chemistry and Chemical Engineering, Xianyang Normal University, Xian Yang 712000, China

[2] *Emerald Experts laboratory, Isfahan Science and Technology Town, Isfahan 84156-83111, Iran*

[3] *School of Chemistry and Chemical Engineering, Queen's University Belfast, Belfast BT9 5AG, Northern Ireland, UK*

*Correspondence to Guang Fan (email: Fanguang179@126.com) and Ahmed I. Osman (email: aosmanahmed01@qub.ac.uk)





## Abstract

MXene-based architectures have paved the way in various fields, particularly in the healthcare area, owning to remarkable physiochemical and electromagnetic characteristics. The modification of MXene structures, along with their combination with polymeric networks, have also gained considerable prominence to further progress their features. The combination of electrospun fibers with MXene faces would be promising in this era since electrospinning has been declared a mature technique that is now being spun out into commercial biomedical applications. The introduction of MXene into the electrospun fibrous frameworks has highlighted outcomes in various biomedical usages, including cancer therapy, controlled drug delivery, antimicrobial targets, sensors, and tissue engineering. Correspondingly, this review describes the employed strategies for the preparation of electrospun configurations in tandem with the MXene nanostructures with fabulous characteristics. Then, the advantages of MXene-decorated electrospun fibers for use in biomedical applications are comprehensively enlightened. According to the investigations, rich surface functional groups, hydrophilicity, large surface area, photothermal features, and antimicrobial and antibacterial activities of the MXene could synergize the performance of electrospun layers to engineer versatile biomedical targets. Also, the future of this path is clarified to combat the challenges related to the electrospun fibers decorated with MXene nanosheets.

**Keywords:** MXene; Electrospinning; Nanofiber; Biomedical application; Drug delivery; Tissue engineering.

## 1. Introduction

In recent decades, nanofibrous configurations have emerged as valuable constraints toward approaching a diverse range of biomedical applications, specifically biomedical targets [1, 2].

View Article Online
DOI: 10.1039/D4NH00209A



Electrospinning is a well-known and scalable technique extensively declared to fabricate flexible fibers in the range of nano to micro diameters with tunable mechanical strength. The electrospun fibers could be feasibly synthesized from numerous polymeric materials in adjustable alignment ratios [3, 4]. Highly porous structure, tiny and interconnected pores, and large surface-to-volume ratio are remarkable characteristics that make the electrospun carrier media a promising candidate for biomedical and tissue engineering applications [5-7]. Meanwhile, several parameters have limited their practical usage, including the challenges linked with the electrospinning procedure in tandem with the defects in the final deployed structures. As an example, several polymers could not be easily fabricated due to improper electric conductivity, low viscosity, or non-electrospinability deportment. Additionally, inhomogeneous structure, poor dimensional stability, inadequate cell infiltration, and cytotoxicity are other unfavorable traits declared for some electrospun compositions [8-10].

As a representational strategy, the addition of nanoparticulate architectures into the electrospun fibers could effectively combat these blocks [11, 12]. The size and distribution of nanoparticles can be effectively modified by adopting appropriate methods of fabrication and carefully adjusting key process parameters [13]. It's crucial to select the right additive with the appropriate morphology and dimensions based on the influencing parameters. In this era, MXene has been broadly investigated for assorted applications, resulting from remarkable features such as electrical conductivity, hydrophilicity, mechanical strength, chemical stability, and high surface-to-volume ratio [14-16]. Besides, photothermal activity, biological features, antimicrobial and antibacterial properties, and formidable adhesiveness to natural organs have caused outstanding outcomes for the MXene-decorated electrospun fibers in biomedical end-users [17, 18].

**Fig. 1a** shows the timeline relating to applying MXene nanosheets in various forms and configurations for tissue engineering targets in the biomedical era. As can be seen, MXene was introduced in 2011 and modified through the years. In 2019, MXene-decorated film was declared as an efficient nanocomposite for bone regeneration [19]. Additionally, loading MXene into the hydrogel [20], 3D printed [21], cryogel [22], and nanofibrous [23] architectures were reported to regenerate bone and heart tissues in 2020. **Fig. 1b** displays the number of Scopus-indexed publications on employing the MXene configurations in various fields, showing the increasing focus on the usage of MXene-loaded structures in different applications. Among various integrated tissue configurations, the electrospun structures have revealed favorable results benefiting the pros of both electrospun media, as well as MXene nanosheets. According to the literature, the MXene nanosheets are commonly embedded into the electrospinning solutions to decorate the electrospun fibers. Based on the polymer chain groups, the MXene galleries could be located inside, on the surface, or in both regions, changing characteristics of the electrospun fibers. **Fig. 1c** exhibits the visualization bibliographic map of the Scopus-indexed papers relating to employing MXene in electrospun structures, highlighting the application of MXene-loaded electrospun structures in a wide range of biomedical usages.

View Article Online
DOI: 10.1039/D4NH00209A



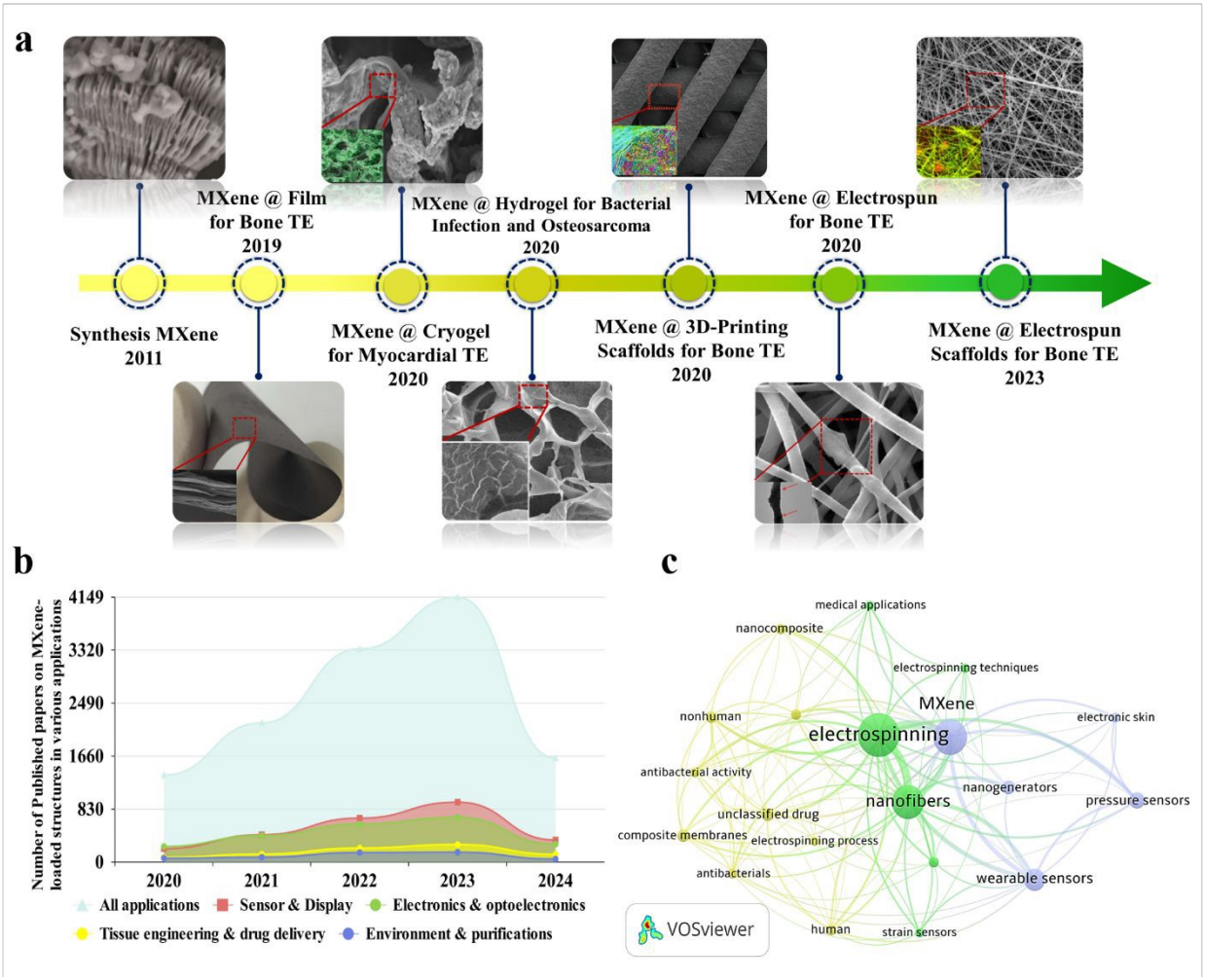


***Figure 1.*** *Evolution history of the MXene-decorated tissue scaffolds; (a) MXene structure: Reproduced from reference [24] with permission from Wiley, Copyright 2011, MXene-loaded film for bone tissue: Reproduced from reference [19] with permission from Dove press, Copyright 2019, cryogen containing MXene for heart tissue: Reproduced from reference [22] with permission from Ivyspring International Publisher, Copyright 2020, hydrogel-based tissue loaded with MXene: Reproduced from reference [20] with permission from the American Chemical Society, Copyright 2020, bone tissue developed by embedding MXene into a 3D-printed layer: Reproduced from reference [21] with permission from Wiley, Copyright 2020, and integrated electrospun fibers fabricated in 2020 and 2023: Reproduced from references [23, 25] with permissions from the American Chemical Society, Copyright 2020 and 2023. (b) the number of Scopus-indexed publications related to the MXene-loaded compositions for various end usages, and (c) visualization of a bibliographic map of the Scopus-indexed papers relating to the usage of MXene in electrospun architectures.*

View Article Online
DOI: 10.1039/D4NH00209A



As a two-in-one strategy, the electrospun architectures integrated with MXene nanosheets have resulted in remarkable compositions applicable to medical-related usages. The synergetic effect of integrating MXene in the electrospun nanofibers for biomedical applications has been overviewed in some studies [26, 27]. Meanwhile, few papers have comprehensively demystified the intriguing behavior of MXene nanosheets, bare electrospun fibers, and MXene-loaded nanofibrous architectures in all biomedical sub-categories. Accordingly, this review has provided an in-depth investigation of the synthesis and characterizing of the MXene nanostructures. Then, the beneficial role of pristine electrospun fibers for biomedical targets is remarked. Additionally, the electrospun scaffolds embedded with MXene nanosheets are overviewed, throwing up many knowledge gaps and novel ideas for exploring versatile electrospun composite networks applicable in cancer therapy, drug delivery, antimicrobial activities, sensor devices, and tissues. Besides, the biomedical usages of the MXene-loaded hybridized structures, obtained through combining the electrospun nanofibers with hydrogels, films, and other polymeric architectures, are pointed out in this review.

## 2. Electrospun fibers for biomedical targets

Polymeric architectures have been extensively declared for various targets in clinical management. To design a fabulous polymeric structure for biomedical applications, the physical features of the polymeric element, in tandem with the geometrical properties, play crucial roles. Chemistry, composition, biodegradation rate, and biocompatibility are categorized as well-documented physical characteristics, while shape and size are critical morphological parameters. In this regard, the selection of polymer type is a significant factor to be noticed. Based on the literature, biopolymers (collagen, gelatin, alginate, chitosan, etc.), polyesters (e.g., polycaprolactone (PCL)), polyamides (e.g., silk and nylon), poly (ortho esters) (e.g., polyglycolic acid (PGA) and poly-lactic acids (PLA)), poly (amido amines), polyanhydrides, and poly (β-amino esters) could be appropriate choices, which are also called bio- and smart-polymers. The polymers, as mentioned above, are hydrolytically degradable and serve prompt physical and chemical changes. The degradability of the polymeric compositions should be customized based on the final usage to prevent the accumulation of materials and so toxicity. Additionally, such polymers are normally selected as they represent proper compatibility with the body. Besides, solubility, thermal stability, mechanical strength, and other inherent features are major properties which are considered depending on the end usage of the designed product [28, 29].

Regarding the geometrical properties, the fabrication of polymeric compositions in the form of thin nanofibers could endow remarkable properties for a wide range of biomedical targets. So far, different mechanical, chemical, thermal, and electrostatic methods have been introduced to generate fine and homogenous fibers in the nanoscale region. Among them, electrospinning has been known as the most employed method as a result of the straightforward setup, which is schematically shown in **Fig. 2**. Electrospinning involves electrohydrodynamic force to form nanoscale threads from polymeric droplets using a high-voltage power supply, a

View Article Online
DOI: 10.1039/D4NH00209A



spinneret, a syringe pump, and a conductive collector. This procedure could be divided into several main steps. In the first phase, the liquid droplet is charged, generating a cone-shaped jet called a Taylor cone. The electric field applied to the droplet induces a charge separation, creating a positive charge at the surface and a negative charge at the center of the droplet. Afterwards, the charged jet is extended along a straight line, forming thin, continuous fibers. The speed and direction of the jet depend on the applied voltage, the distance between the spinneret and the collector, and the solution properties, such as viscosity and surface tension. Then, the jet thins out due to the presence of an electric field and grows the electrical bending instability, which arises from the competition between the electrostatic repulsion and the surface tension of the jet. As a result, the jet meanders and forms a series of loops and coils, leading to an increase in the surface area of the fibers. Finally, the jet solidifies and forms nanoscaled fibers, which are gathered on a collector. The collected fibers can be further processed by annealing, crosslinking, or functionalization to enhance their mechanical, chemical, and biological properties [30-32].

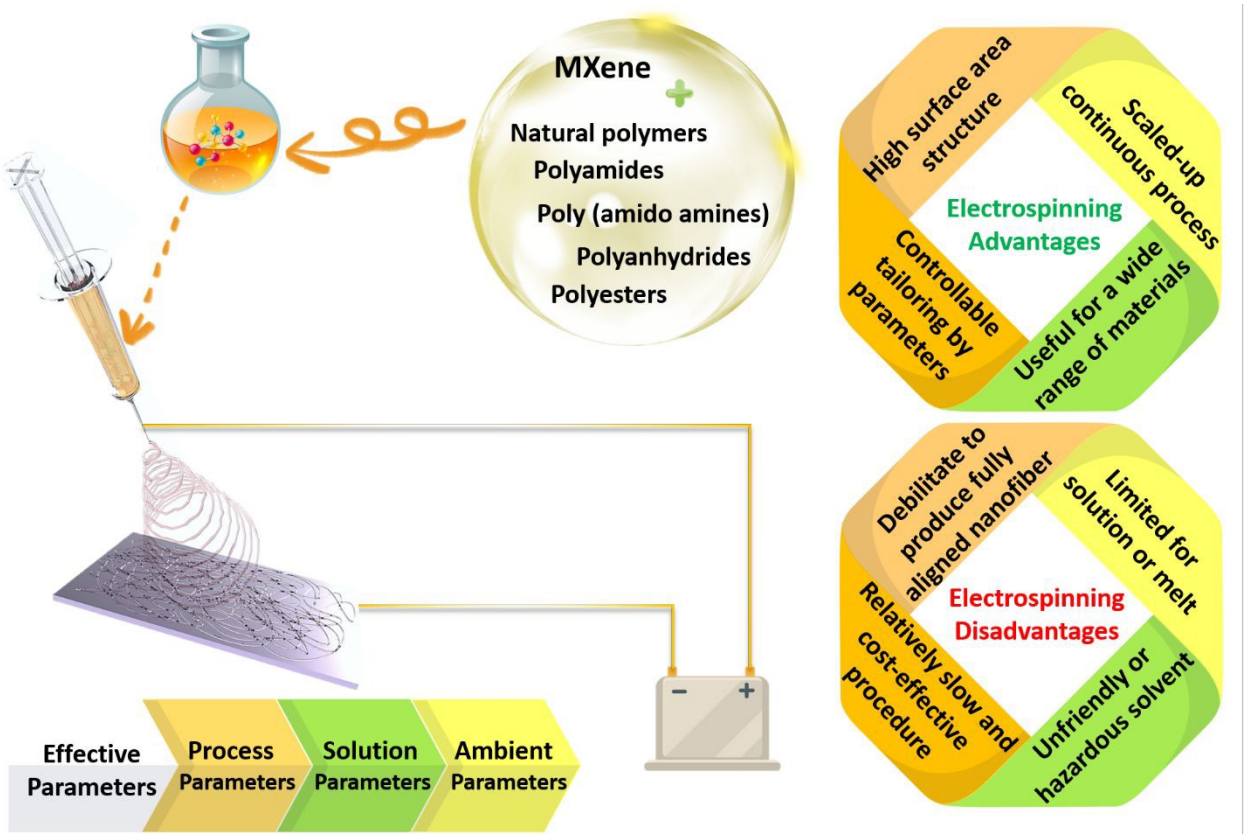


***Figure 2.*** *Schematic illustration of the electrospinning setup, along with the pros and cons of the electrospinning method for the fabrication of nanofibrous structures.*

The electrospinning process could be modified by playing with electrospinning parameters, such as the solution factors, in tandem with the electrospinning conditions, leading to fabricating fibrous structures with various morphologies. For example, the critical voltage employed during the electrospinning is identified based on the polymer solution. Changes in the critical voltage of a specific electrospinning solution could lead to fibers with different

View Article Online
DOI: 10.1039/D4NH00209A



morphological structures being obtained. In this era, a proper voltage range of 10-20 kV was exhibited for electrospinning the PAN nanofibers. According to this study, a rise in the voltage from 10 to 20 kV could cause the formation of finer fibers due to the amplified repulsive forces, thereby inducing more stretching [33]. However, increasing the voltage might fabricate fibers with larger diameters in some cases. For example, Matabola et al. [34] declared an increment in the average PVDF fiber diameters from 100 to 180 nm by enhancing the voltage from 10 to 16 kV. There is also a critical flow rate for electrospinning the polymer solutions, varying based on the polymer type, in tandem with solution concentration. Generally, the flow rate differs from a hundred microliters to a thousand microliters per minute in standard polymer solutions. A rise in the optimized range of the feeding rate could lead to generating thicker fibers, resulting from the ejection of more solution. For example, a shift from 1 to 2 $\mu l.min^{-1}$ in the feeding rate increased the fiber diameters from 18.9 to 36 µm. It is worth noting that an asymmetrical Taylor cone is developed below the optimized threshold, causing instability of the electrospinning jet and the fabrication of fibers in a wide-diameter distribution [35]. As another variable, the working distance should be set based on the polymer system to attain homogenous electrospun fibers. In short working distances, solvent evaporation is limited, leading to defects and beading in the nanofibers. Also, the electrical field is weakened above the threshold, increasing the jet instability. In a study conducted by Jabur et al. [36], it was displayed that a rise in the working distance from 4 to 22 cm could lead to an increase in the PVA fiber diameters from 875 to 600 nm. Therefore, it is vital to determine the optimized parameters based on the required morphological factors of the electrospun fibers.

Electrospun fibers have shown several advantages, including a high surface-to-volume ratio, consistent structure, tunable porosity, and malleability to conform to diverse sizes and forms. These characteristics make electrospun fibrous membranes particularly attractive for biomedical applications, such as cancer therapy, drug delivery, sensor devices, and tissue engineering. In drug delivery systems, high surface area is beneficial as it allows for loading diverse amounts of drugs. Additionally, loading larger therapeutic agents into the system becomes more accessible with an expandable pore size. It is important to note that the specific surface area of a drug delivery system has a significant impact on the rate of drug release. This is because the surface area determines the amount of drug that is exposed to the surrounding environment and thus controls the rate at which the drug is released [37, 38].

Also, electrospun membranes have established specific attention in generating biosensors due to showing a high surface area, modification simplicity, and fabricability. Additionally, nanosized structures have proven effective as membranes that immobilize bioanalytics. This creates a favorable microenvironment for physiologically active molecules, enhancing biosensing efficiency [39-42]. In the case of tissue engineering, the high surface-to-volume ratio allows for increased cell attachment and proliferation, while the consistent structure provides a uniform environment for tissue growth. Furthermore, electrospun fibers' tunable porosity and malleability permit customization to match specific application requirements.

View Article Online
DOI: 10.1039/D4NH00209A





However, this technique still faces two main limitations: insufficient tiny pores and porosity and poor mechanical properties, which are significant features that cover the requirements essential for biomedical applications [31]. To overcome the challenges, researchers have come up with some innovative solutions. One approach is to adjust the electrospinning parameters, such as the solution concentration, flow rate, applied voltage, and the collector. Accordingly, numerous attempts have been devoted to optimizing the fiber diameter, pore size, and porosity of the electrospun fibers. As an example, McCann et al. [43] utilized a cryogenic liquid to collect the fibers. In the proposed procedure, a phase separation was induced between the solvent and the polymer, forming highly porous structures and revealing a promising architecture for various biomedical applications. Another approach is to use a sacrificial component during electrospinning, which can be removed to create a more open and interconnected network for cell migration. Considering this strategy, Huang and Thomas combine chloroform with ethanol and dimethyl sulphoxide as low and high boiling point liquids to create surface and internal porosity in the electrospun PLA nanofibers, respectively [44].

Poor mechanical strength is another challenge related to the electrospun networks for load-bearing applications. Therefore, post-processing modification techniques, such as cross-linking, annealing, or heat treatment, have enhanced the structural and mechanical strength of electrospun fibers. These approaches could create fibrous membranes that are more suitable for biomedical applications and tissue engineering targets [45-47]. For example, Lee et al. [48] Utilized a simple freezing/thawing process to increase the crystallinity of the PVA electrospun fibers from 23.5 to 43.6%, thereby raising the mechanical strength to 65% compared to the untreated PVA nanofibers.

Additionally, integrating particulate fillers into the electrospun structures has been extensively recommended as an efficient modification [49, 50]. For example, carbon nanotubes (CNTs) and graphene are documented as appropriate fillers for the polymeric membranes, which could be evenly distributed in the developed architectures. The high mechanical strength of the CNT filler could provide incomparable superb specific strength for the electrospun fibers [51]. The enhancement of mechanical strength in the CNT-loaded electrospun fibers could be attributed to the increased interconnections between the polymer chains by the presence of CNT filler. Also, the mediated CNT could decrease the contact angle and improve cell viability in the electrospun tissues [52]. However, graphene has been known as a more interesting filler for promoting the characteristics of electrospun fibers due to its abundance and lower cost [53]. Reduced graphene oxide (rGO), a substantial graphene derivative, has been widely employed to engineer potential bioactive electrospun architectures. While GO possesses frequent functional groups, and so proper hydrophilicity, rGO provides superior electrical conductivity [54]. Accordingly, Ivanoska-Dacikj et al. [55] declared that the incorporation of 20 wt. % rGO into the PEO-based nanofibers could effectively reduce the electrical resistance, leading to an approach of 96% cell viability. In another attempt, Gozutok et al. [56] displayed that the incorporation of 1 wt.% rGO into the PVA nanofibers could serve 23 and 30% higher elastic

View Article Online
DOI: 10.1039/D4NH00209A

modulus and tensile strength values than those of the neat PVA nanofibers, resulting from the created strong interaction between the PVA polymer chains and rGO nanogalleries. Moreover, TGA analysis confirmed the thermal degradation of rGO-filled PVA structure at $450^0$C, while the pure PVA fibers degraded at $345^0$C. Furthermore, the filler incorporation led to an increment in the electrical conductivity from 0.1 to 11 $\mu S.cm^{-1}$.

As a new emerging filler, MXene nanosheets have also reaped much attention by boosting the mechanical properties, along with enhancing the physiological and biological features, widening their applications in various biomedical fields. MXene nanosheets could be easily embedded into the electrospinning solutions and form thin nanofibers, benefiting from their outstanding rheological characteristics. These structures endow excellent electrical conductivity with no need to perform reduction procedures. MXene-loaded solutions could be generated in various cylindrical, ribbon, aerogel, or core-shell structures, depending on the polymer matrix. The defects and loose stacking states of the MXene-integrated electrospun fibers could be enhanced by the axial MXene orientation in the electrospun networks. By tuning the spinning condition, MXene size, and filler concentration, different physical, chemical, mechanical, and electrical conductivity could be tailored depending on the considered application. Correspondingly, the MXene-polymer nanofibers composite has convincingly shown tremendous potential in promising areas, such as antibacterial treatments, wound healing, cellular differentiation, bone tissue regeneration, neural tissue guidance, and health monitoring systems. In the following section, the role of MXene in biomedical applications is described based on its noteworthy properties.

## 3. Synthesis methods and biomedical applications of MXene

### 3.1 Synthesis and Characteristics of MXene

Over the last two decades, two-dimensional (2D) nanomaterials have been an attractive field of study due to their outstanding physical and chemical properties. Carbides and nitrides of early transition metals are considered significant materials, resulting from their unique features consisting of superior chemical stability, excellent hardness, and high metallic electrical conductivity [57]. MXenes are 2D inorganic compounds with few atoms thickness, comprising nitrides, carbides, and carbonitrides layers of early transition metals [58]. MXenes are usually obtained by chemical etching of a MAX phase with a general formula of $M_{n+1}AX_n$, where M represents an early transition d-metal (Mo, Ti, Zr, Cr, etc.), A is mostly referred to as an element of group 13 to 16 (e.g., Al, Ga, Ge, Si, etc.), X represents carbon and/or nitrogen, and n is equal to 1 to 3 (see **Fig. 3a**). The MAX phase possesses a layered hexagonal structure, including densely packed M layers and X atoms occupied octahedral positions. After selective etching of A layers in the MAX phase, the chemical formula of resulting MXene would be $M_{n+1}X_nT_z$, where $T_z$ is the surface terminations group (–F, –O, –OH, etc.) bonded to M, and z is the number of the interfacial functional groups [59].


View Article Online
DOI: 10.1039/D4NH00209A



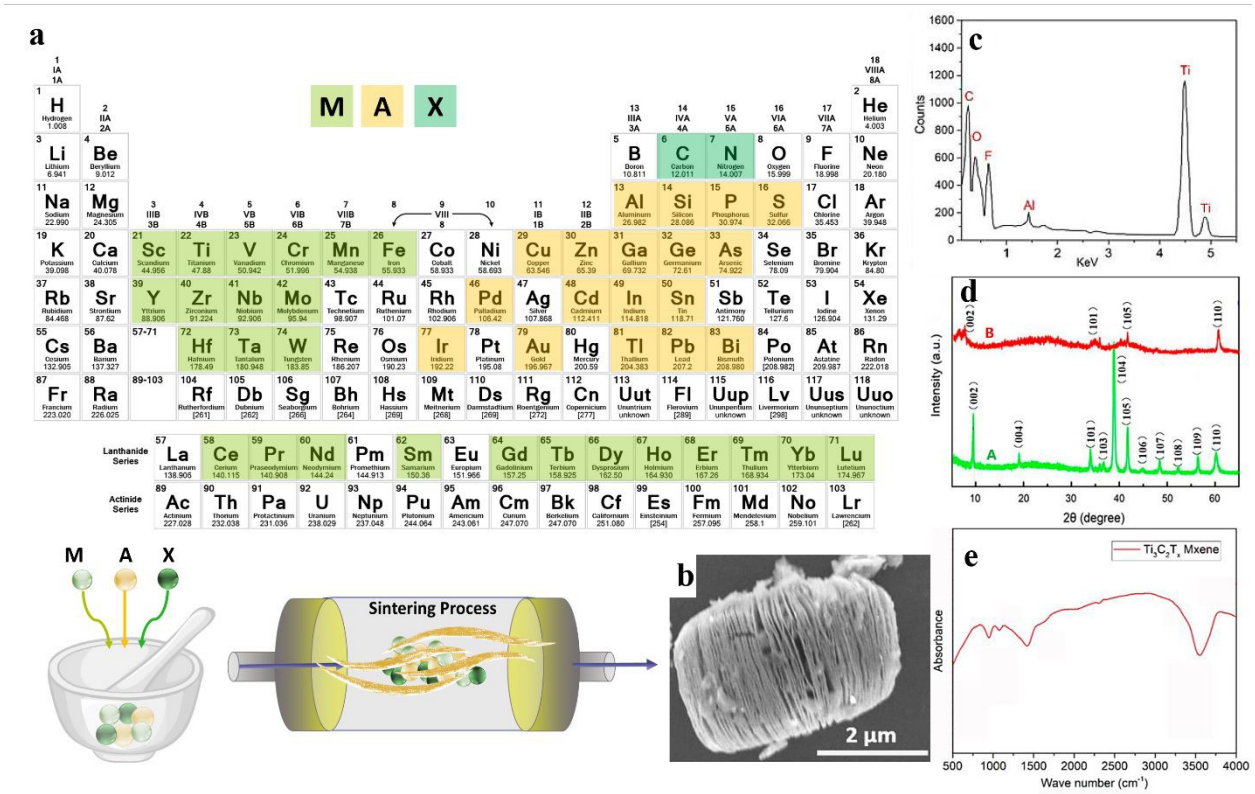


***Figure 3.*** *The structure and synthesis of the MXene nanosheets; (a) schematic illustration of the MXene structure and synthesis procedure. (b) SEM, (c) EDX, (d) XRD, and (e) FTIR results of the $Ti_3AlC_2$ and $Ti_3C_2T_x$ powders, Reproduced from reference [60] with permission from MDPI, Copyright 2020.*

To date, several attempts have been devoted to developing the etching methods. In general, these approaches could be divided into three different methods, including wet chemical, molten salt, and electrochemical methods [61]. Among them, the wet chemical etching route is the most conventional and mature etching technique, consisting of HF-containing and HF-free approaches. Although it is reported that HF-containing methods possess high-risk operation conditions and require extra caution, it is still the most efficient etching technique [62]. Accordingly, studies over wet chemical routes to minimize or even avoid using HF resulted in valuable outcomes. As an example, Dirscoll's group reported using a small portion of HF along with other acids. They successfully fabricated $Ti_3C_2$ MXene using a volumetric ratio of 6:3:1 of HCl: water: HF [63]. Comparing the conventional use of HF as the etchant, the proposed method reduced the usage of this hazardous acid by 90%. Additionally, the authors reported fewer structural defects, large lateral sizes, and high yield for the developed MXene nanosheets. In another approach, $Ti_3C_2T_x$ was synthesized by immersing the $Ti_3AlC_2$ powders in a LiF/HCL solution. SEM illustration of the synthesized nanosheet is displayed in **Fig. 3b**. Additionally, the elemental mapping of the generated nanostructure is represented in **Fig. 3c**, showing strong peaks of C, Ti, O, and F components, along with a weak peak regarding the Al

View Article Online
DOI: 10.1039/D4NH00209A

element. Accordingly, the etching procedure was almost completed in the obtained MXene nanostructures. Also, the presence of –F, –OH, and –COOH functional groups could be corroborated by the appeared peaks. **Fig. 3d** examines the XRD patterns of the $Ti_3AlC_2$ and $Ti_3C_2T_x$ powders. As can be seen, the $Ti_3AlC_2$ revealed about eleven peaks, showing its crystalline structure. Meanwhile, the crystalline regions were reduced to 4 phases after the etching procedure, which could be linked to the removal of Al layers. The 002 crystalline plane was also shifted to a lower value in a broadened peak, proving a rise in c-spacing by replacing the Al atoms with –F and –OH functional groups. **Fig. 3e** shows the FTIR spectrum of the $Ti_3C_2T_x$ nanosheets, displaying the –OH and C–F vibrations at 3490 and 1216 $cm^{-1}$, respectively [60].

The molten salt etching is based on the selective removal of A elements through a redox reaction of molten salts and A elements. Consequently, it can be used to install and remove surface functional groups. Moreover, applying molten salts as etchant enables synthesizing MXenes with –O, –S, –NH, –Se, –Cl, and –Br termination, as well as bare MXenes with no surface group [64]. As an example, Urbankowski et al. [65] employed this method to synthesize the first nitride MXene $Ti_4N_3T_z$. Additionally, Huang et al. [66] applied molten $ZnCl_2$ for the etching of new Zn-MAX phases, such as $Ti_2ZnN$, $Ti_2ZnC$, $Ti_3ZnC_2$, and $V_2ZnC$, reporting the substitution of Zn and resulting Cl-terminated MXenes.

The electrochemical etching method has also been used as an effective route to fabricate MXenes in an HF-free way [64]. $Ti_2CT_z$ and $Ti_3C_3T_z$ can be obtained through electrochemical etching of A elements from $Ti_2AlC$ and $Ti_3AlC_2$ MAX phases using HCl, $NH_4Cl$, and tetramethylammonium hydroxide as an electrolyte. However, extreme etching would change the MAX phase to carbon as a result of the simultaneous dissolution of A and M fundamentals [67]. Apart from the aforementioned etching methods, some other infrequent approaches have been used. A promising study by Yang et al. [68] reported the anodic corrosion of $Ti_3AlC_2$ as a fluoride-free etching process. The authors claimed that the method successfully transforms $Ti_3AlC_2$ to $Ti_3C_2T_x$ with a sufficient yield.

In the generated multilayered MXene structures, the layers are held together through van der Waals and hydrogen bonding. Nevertheless, these secondary bonds make the intercalation between layers possible to produce delaminated MXene [69]. Generally, inorganic cations and organic or ionic compounds are utilized for the intercalation and, thereafter, an ultrasonication step. Due to the negatively charged surface of the as-obtained flakes, they are able to make a stable suspension in organic solvents or water without any surfactant addition. Based on the literature, several cations, such as Na(1+), K(1+), Mg(2+), and Al(3+), have been successfully applied to intercalate the MXenes [70]. As a result, MXenes can be obtained in different forms of multilayer powders to delaminated flakes, which can be employed in several applications via various techniques, including printing, spraying, fiber forming, electrospinning, and many more [58].

MXene structures could be feasibly functionalized with covalent and non-covalent bond interactions to combat the MXene weak points, such as poor oxidation stability. Non-covalent

View Article Online
DOI: 10.1039/D4NH00209A





functionalization is commonly carried out through weak intermolecular or interatomic bonding, such as van der Waals forces, hydrogen bondings, or electrostatic interactions in a fast and mild procedure. Meanwhile, the covalent functionalization method creates strong interactions via equal sharing of electron pairs, offering surface modification with superior stability. Unlike the non-covalent modification method, covalent functionalization requires a complex synthetic procedure, lasts long, and might lead to oxidative degradation [71, 72]. Overall, far from synthesizing other 2D materials with similar applications that yield small amounts under challenging conditions, MXenes can be produced on a large scale through a straightforward procedure, making it more potential to meet industry measurements. MXenes have become one of the most favorable groups of 2D nanomaterials because of their outstanding properties. The easy functionalization of MXenes renders them extremely auspicious material for laboratory studies, as well as practical usage in various industries.

## 3.2 The role of MXene and MXene-loaded nanofibers in biomedical applications

According to the literature, the MXene family is a promising candidate to boost versatile structures for a wide range of applications, such as environment and purification, electronics, sensors and displays, and biomedical targets. In the biomedicine category, MXene has been utilized to optimize the efficiency of cancer treatment, drug delivery, bioimaging, and biosensors in the developed architectures. The highlighted potentials could be referred to as proven fascinating features of the MXene-based configurations, such as proper elastic mechanical strength, electronic conductivity, hydrophilicity, chemical stability, and many more [73]. Incorporating MXene nanosheets into the electrospun fibers creates a synergetic effect for biomedical applications due to their complementary features. The combination of MXene layered structure and high porosity of electrospun fibers endow a large surface area. The mechanical strength of the electrospun fibers could be reinforced by embedding the MXene nanosheets into the nanoarchitecture, attesting to better performance in various biomedical applications. The layered structure of the MXene, in tandem with appropriate morphological characteristics of the electrospun fibers, serves great capacity for loading drugs, providing sustained and controlled drug release. The electrical conductivity could also be escalated by incorporating the MXene into the conductive electrospun fibers, which is favorable for tissue engineering and sensors.

### 3.2.1 Cancer Therapy

In recent years, the MXene family has been introduced to achieve therapeutic, imaging, and drug delivery precise abilities in photothermal tumor treatments (PTT) and photodynamic therapy (PDT). High light-to-heat conversion efficiency and strong absorption in both the first and second NIR bio windows in comparison with conventional photosensitizers, have remarked the advantages of MXene nanostructures toward PTT and PDT. Also, the highlighted capabilities of MXenes in anti-cancer therapy could be linked with the proper atomic number, paramagnetic behavior, and high surface-to-volume ratio. Common cancer therapies lead to unwanted side effects and drawbacks, resulting in direct biological targeting for the local cancer treatment requiring signal transduction and actuation, which could be carried out via radical oxygen, heat, and irradiation. Among the introduced methods, PTT is assumed to be a fresh and efficient

View Article Online
DOI: 10.1039/D4NH00209A

treatment for cancer curing. In this technique, the light is converted to heat, causing cell death without influencing the surrounding tissues. Also, the precise location of the cancer cells could be detected and monitored through the PTT agent inflation in tumors in a remotely controlled manner.

Li et al. [74] utilized a droplet light heating system to estimate the light-to-heat photothermal activity of the $Ti_3C_2$ MXene nanostructure. A wide spectrum laser beam was irritated to the droplets containing $Ti_3C_2$ and CNT, implying a higher temperature for the $Ti_3C_2$ than that of the CNT, possibly due to the superior light absorption of the MXene. According to the obtained data, excellent light absorption capability was represented by the employed $Ti_3C_2$ compared to that of the carbon nanotubes. Accordingly, the CNT structure did not reveal any absorption peak from 300 to 1300 nm, while $Ti_3C_2$ showed a higher absorption and an observable peak around 800 nm. In addition, the internal light-to-heat conversion efficiency of 100% was approached. Despite the great advantages of MXene, its non-stable structure in buffer saline, poor oxidation stability, and agglomeration behavior have motivated researchers toward modifying the MXene family through combination with other structures. Gao et al. [75] designed a 3D honeycomb structure comprising $Ti_3C_2$/CNT to approach the anti-aggregation property, displaying proper photothermal activity and stability in the NIR region.

It is also worth noting that among various 2D materials, MXene nanosheets are ideal for use in PDT as photosensitizers. PDT is a safer and more targeted cancer treatment than chemotherapy and radiotherapy, reducing the risk of side effects [76]. This is because photosensitizer drugs only become toxic when activated by external light. In this era, Liu et al. [77] confirmed the excellent drug release profile of MXene-based structure, due to its efficient NIR laser-induced and pH-responsive behavior. The attempts in the area of MXene modification in cancer therapy have resulted in the evaluation of MXene photothermal activity in different configurations, including $Ti_3C_2$ quantum dots [78], $Ti_2C$ nanosheets [79], $Ti_3C_2$/Co nanowires [80], MXene/Doxjade platform [81], Au/$Fe_3O_4$/$Ti_3C_2$ nanocomposite [82], MXene/PVA hydrogel [83], collagen/silk/hydroxyapatite/MXene 3Dprinted scaffold [84], MXene/borneol-poly(N,N-dimethyl ethyl methacrylate) [85], and many more. Furthermore, MXene-based nano/microarchitectures could be employed in targeted anti-cancer drug delivery systems or therapeutic agents after modifying with biocompatible activated agents. Considering the beneficial characteristics of the electrospun fibers in biomedical engineering, as well as the prominent role of MXene in designing versatile architectures, several studies have been devoted to analyzing the properties of the MXene-loaded electrospun compositions. For example, Ding et al. [86] declared that simultaneous $Ti_3C_2T_x$ electrospray on the $Ti_3C_2T_x$-loaded PLA nanofibers could generate a highly efficient membrane with the ability to kill tumor cells, in tandem with bacteria after surgical melanoma excision, decreasing the tumor recurrence. **Fig. 4a** shows the SEM image of the electrospun fibers decorated with MXene nanocoating. **Fig. 4b** exhibits the upper and lower surfaces of the provided films attached to the hot plate. When the hot plate was applied to the upper surface, the lower surface of the sample containing MXene nanosheets represented higher temperature compared with that of the free-filler film, corroborating the better

View Article Online
DOI: 10.1039/D4NH00209A



conductivity of the MXene-loaded film. Resulting from the $Ti_3C_2T_x$ presence both inside and on the surface of the electrospun fibers, and so an excellent unidirectional thermal conductivity, a high temperature of about 70℃, could be achieved in 1 min with proper photothermal cycling stability. As a result, reaching a certain temperature in the developed structures could result in killing the B16F10 cancer cells. **Fig. 4c** shows the tumor growth curve relating to the application of various films. Based on the results, the tumor recurrence was effectively prevented from MXene-loaded structure. Additionally, an antimicrobial ring diameter of 1.3 cm was approached in the mentioned membrane under 808 nm laser NIR light, mighty resulting from the enhanced thermal distribution in the lower surface of the fibrous structure.

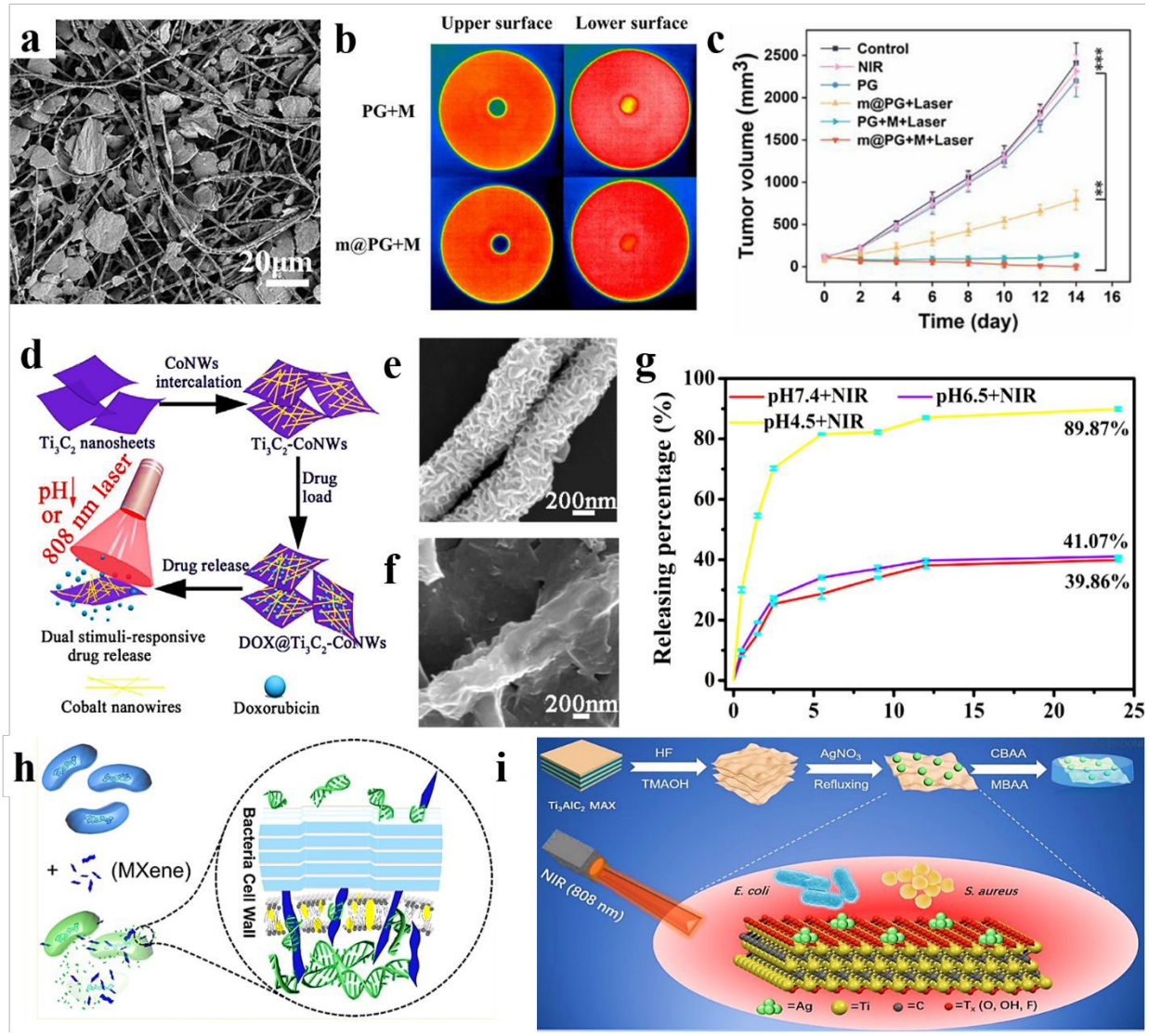


***Figure 4.*** *Characteristics of the PLA nanofibers decorated with electrosprayed MXene for cancer treatment; (a) SEM image of the film, (b) temperature distribution in the MXene-free and MXene-loaded films, and (c) the growth curve of tumor volume in different provided films. Reproduced from reference [86] with permission from Elsevier, Copyright 2023. Properties of the $Ti_3C_2$/cobalt nanowire heterostructure; (d) the designed procedure, (e&f) SEM images of the*

View Article Online
DOI: 10.1039/D4NH00209A

*$Ti_3C_2$ and $Ti_3C_2$/cobalt nanostructures, and (g) drug delivery rate. Reproduced from reference [80] with permission from Elsevier, Copyright 2020. (h) Mechanism of the MXene antimicrobial activity. Reproduced from reference [87] with permission from the American Chemical Society, Copyright 2018. (i) Simultaneous use of antimicrobial and NIR photothermal activities of MXene/Ag nanocomposite. Reproduced from reference [88] with permission from the Royal Society of Chemistry, Copyright 2020.*

### 3.2.2 Drug delivery

Ultra-thin 2D planar structure, NIR responsiveness, photothermal conversion capability, and chemically adjustable surface functionalities of the MXene family caught the interest of researchers for developing efficient controlled drug release systems. MXene structures could more freely migrate through the body than the large particles. In addition, a lower drug amount is required to be loaded on the MXene due to its outstanding surface area. Notably, the pH sensitivity and photothermal activity of MXene structures have made them a great candidate in cancer therapy. Therefore, these unique materials could reveal a dual-stimuli response for drug release, as well as ablation of malignant cells.

Although the MXene family has revealed remarkable characteristics, their inadequate control ability and poor drug loading capability lead to continuous drug detaching and injuring normal tissues. In addition, non-stable structure in the physiological conditions causes the limitation toward efficient treatment of cancer diseases. To address the highlighted downsides, adding magnetic nanoparticles to the MXene structure has been considered a prominent strategy [89, 90]. Accordingly, the drug could be effectively confined to the targeted tissue by applying an external magnetic field. For example, Liu et al. [80] designed a heterostructure $Ti_3C_2$ MXene/cobalt nanowire, noticing the ferromagnetic properties of the cobalt. In this study, the cobalt is intercalated on the $Ti_3C_2$ nanosheets, and the doxorubicin was loaded on the prepared structure. Then, the loaded drug was released under an 808 nm laser beam in three pH levels, which is schematically summarized in **Fig. 4d**. SEM images of $Ti_3C_2$ and $Ti_3C_2$/cobalt nanocarriers are illustrated in **Figs. 4e&f**, respectively. The provided structure showed excellent photothermal conversion activity at the wavelength of 808 nm. The doxorubicin loading increased up to 225%, corresponding to the electrostatic interaction between the negative surface of the $Ti_3C_2$-cobalt nanocarriers and the positive charge of the employed drug. In addition, the drug release of the prepared material in various pHs is shown in **Fig. 4g**, declaring 89.3% release at a pH of 4.5 after illuminating NIR for 24h. Overall, chemo photothermal therapy could be enhanced resulting from the synergetic effects of the composite elements, which is beneficial in cancer therapy.

MXene properties could also be modified by various polymers. For example, hydrophobic biocompatible polymers, such as PLGA, can tune the hydrophilicity inherent feature of the MXene and ease its interaction with hydrophobic drugs [91]. In addition, the combination of photothermal polymers, such as polypyrrole and polydopamine, can cause a synergetic effect and

View Article Online
DOI: 10.1039/D4NH00209A



boost the MXene performance. Moreover, polymer matrixes could provide a desirable accommodation for the MXene nanoparticles, impeding the leakage in the body [92]. In this era, the enhanced drug delivery performance of MXene combined with nanoscaled polyacrylamide [89], polyethylene glycol (PEG) [93], Chitosan/hyaluronic acid/gold [94], agarose [95], polydopamine/gold [96], and PEG/gold [97] compositions are reported.

To escalate the efficiency of drug delivery systems, temperature-responsive MXene nanobelt fibers were generated through electrospinning the PAN/PVP/MXene solution, followed by coating with polyacrylonitrile and polyvinylpyrrolidone composition. In a 3 min time, the developed structure could reach from 23 to 39$^0$C under NIR exposure. Accordingly, the coating layer could be opened and the loaded vitamin E could be released in a favorable profile over a longer period, resulting in good wound healing. According to the obtained data, proper surface area, high mass loading, and the mass production capability of the suggested structure could facilitate the application of this architecture in a diverse range of biomedical applications, from drug delivery and wound dressing to biosensors and tissue engineering [98]. In another research study, a hybrid system was designed comprising MXene nanofibers and hydrogel components embedded with deferoxamine mesylate (DFOM) and acetylsalicylic acid (AC) to develop a highly efficient wound dressing. Based on the results, the photothermal activity of the MXene nanofibers could regulate the release of DFOM to prevent excessive angiogenesis. The immune micro-environment around the wound region could be controlled by favorable release of AC, assisting in approaching appropriate anti-inflammatory activity [99].

### 3.2.3 Antimicrobial activity

Today, medication overuse has caused microorganism resistance against drugs' antimicrobial activity, requiring the development of materials with superior efficiency. MXene family possess a remarkable antibacterial property, linked with appropriate semiconductor features, hydrophilicity, electrical conductivity, functional groups on the surface, the thickness of the atomic layer, and optical behavior (see **Fig. 4h**). Based on the literature, these materials are able to inhibit Gram-negative (E. coli) and Gram-positive (B. subtilis) growth, depending on the employed MXene concentration. This could be attributed to the interfacial interaction between the MXene-based structures and the cells. In fact, this direct contact destroys the cell membranes, followed by cell death. The active surface, as well as the small size of the MXene nanosheets, ease their penetration into the cells, resulting in their significant interaction with the specific molecules placed in the microbial cell walls and cytoplasm, and eventually, cell disruption and death. Moreover, a conductive bridge could be created on the lipid layers due to the anionic surface of the MXene nanostructures, boosting the electron transduction from bacteria to the environment and so the cell death [100, 101]. Furthermore, the hydrogen bonding between MXene's surface functional groups lipopolysaccharide string in the cells might hinder bacterial growth. As an example, better antimicrobial behavior was reported by reducing $Ti_3C_2T_x$ nanosheet size against both E. coli and B. subtilis [102]. In another attempt, the application of $Ti_3C_2T_x$ was proposed to attain both photothermal and antibacterial activities, which is schematically depicted in **Fig. 4i**. [103].

View Article Online
DOI: 10.1039/D4NH00209A



Benefitting the favorable characteristics of the electrospun fibers, a core-shell structure was generated comprising PCL/$Ti_3C_2T_x$ and PCL/gelatin/$Ti_3C_2T_x$, respectively, as the core and shell to develop an antibacterial and electroactive wound dressing. Based on the results, the presence of $Ti_3C_2T_x$ led to an increment in the mechanical stability, antibacterial behavior, proliferation activity, and wound healing procedure. Additionally, the electrospun matrix acted as a barrier against bacterial infiltration through the formation of a dense structure, revealing a promising architecture applicable in bioactive dressings for cutaneous wound healing [104].

### 3.2.4 Smart sensors

The large surface area and easy surface modification ability of the MXene groups potentiate them for application in the design of various sensors, such as gas, humidity, stress-strain, and optical devices. In addition, the ideal MXene properties, such as biocompatibility, conductivity, surface chemistry, and shaping, have made it an exceptional platform for electrochemical sensors [41, 105]. Besides, MXene nanosheets have illustrated a wide band gap. For instance, the band gap of some MXenes Oxides, such as $Zr_2CO_2$ and $Ti_2CO_2$ is found to be 2.13 and 1.15 eV, respectively. Moreover, when compared to other established 2D nanomaterials like graphene, MXenes propose superior hydrophilicity and superior electrical conductivity [106, 107]. Furthermore, studies have shown higher electrical conductivity of MXene nanosheets compared with CNTs and reduced graphene oxide (rGO) materials, which could be attributed to their layered structure, allowing for efficient electron transport along the layers [74, 108]. Accordingly, such structures could be employed in chronoamperometric biosensors due to its unique characteristics, including electrocatalytic activity and fast response in the 50 to 750 μm region, which is beneficial for glucose detection. Meanwhile, van der Waals bondings between the MXene sheets cause the synthesis of thin layers and nanosheet aggregations, requiring further modification methods to address the block as mentioned above [109-111]. As an example, Rakhi et al. [112] developed a $Ti_3C_2T_x$/Au composite for glucose biosensors, showing proper stability and reproducibility behaviors. MXene-based materials have also illustrated a prominent role in fabricating wearable electrochemical sensors, applicable in health- and sport-related devices. Accordingly, a porous sandwiched structure was fabricated comprising $Ti_3C_2T_x$ and PLA to produce a pressure-flexible and degradable sensor, representing a great sensitivity even in a wide range from 10.2 Pa to 30 kPa and great cyclability over 10000 cycles. So, it could be utilized in monitoring the patient's health effectually and in real-time clinical diagnosis [113]. In an attempt carried out by Sohel Rana [114], it was declared that loading $Ti_3C_2T_x$ nanosheets into the PVDF-TrFE nanofibers could generate a sensor motion with outstanding low-pressure performance (power 4.02 W/m2) as well as proper mechanical response sensitivity (1.1 V/kPa). According to the results, embedding $Ti_3C_2T_x$ could cause a rise in the electronegativity, dielectric property, and biocompatibility of the provided architecture, resulting from the formation of microscopic dipoles and microscopic networks. Hence, the integration of electrospun fibers with MXene-based galleries could open a viable new avenue to tackle challenges in sensor fabrication and approach the desirable performances.

View Article Online
DOI: 10.1039/D4NH00209A

### 3.2.5 Tissue engineering

The organs' injuries and fractures could result in traumas, diseases, paralysis, and mortality of many people every year. The multifaceted tissue engineering field has utilized biomaterials, biological molecules, cells, and scaffolds to efficiently recover and reconstruct damaged organs. Accordingly, numerous attempts have been made to design tissues with the ability to mimic natural matrixes. Therefore, novel composite scaffolds have been developed, comprising synthetic and natural polymers, as well as ceramics and 2D materials. MXene is a considered 2D geometry substance, endowing notable characteristics to the scaffolds due to its large surface area, proper hydrophilicity, 2D structure, conductivity, and particle size regulation. The hydrophilic surfaces of MXenes, with high metallic conductivities, distinguish them from most 2D materials such as graphene. Moreover, their high metallic conductivity allows them to efficiently transport electrical signals, which is crucial for many tissue engineering applications [115]. Meanwhile, more attempts are required to optimize and adjust the prepared composite according to the targeted native matrix, such as oxidative stability, biodegradability, biocompatibility, physiological condition stability, etc. Correspondingly, surface functionalizing of the MXene by organic and inorganic materials has been extensively suggested as a result of its high surface area. Also, the formation of MXene in various composite architectures, such as membranes, layers, porous structures, particles, 3D printed composites, and specifically nanofibrous configurations, could integrate its features.

MXene-based structures have been employed to boost the regrowth and reconstruction of various tissues. For example, it is a good choice for designing and regeneration of bone defects. The MXene-based materials easily interact with water and oxygen, causing their degradation and subsequent release of Ti-based materials. Such species are appropriate for the promotion of bone cell growth. Therefore, they could be applied in bone cancers to simultaneously ablate the tumor cells and reconstruct the bone. Pan et al. [17] synthesized a 3D-printed $Ti_3C_2$/bioactive glass bone scaffold (TBGS) and compared it with a bioactive glass 3D-printed membrane (BGS), which is a common and beneficial material for bone scaffolds. The fabrication route of both BGS and TBGS layers are schematically provided in **Fig. 5a**. A desirable element distribution was also shown by the element-mapping analysis (See **Fig. 5b**). As is depicted in **Fig. 5c**, triggering photothermal ablation was examined by irradiating the osteosarcoma cells by 808 nm laser. **Fig. 5d** confirmed much fewer living cells with increasing the laser-irradiation duration. 3D reconstruction of the tissue was analyzed after 24 weeks of implantation of the composite scaffolds, representing more calcified tissues and better regeneration outcome with the presence of TBGS, compared with that of applying BGS (**Figs. 5e**). The values of BV/TV, BMD, and TOT in newborn osseous tissues collectively exhibited a superior osteogenic performance of TBGS than the BGS layer, displaying in **Figs. 5f-h**.

View Article Online
DOI: 10.1039/D4NH00209A



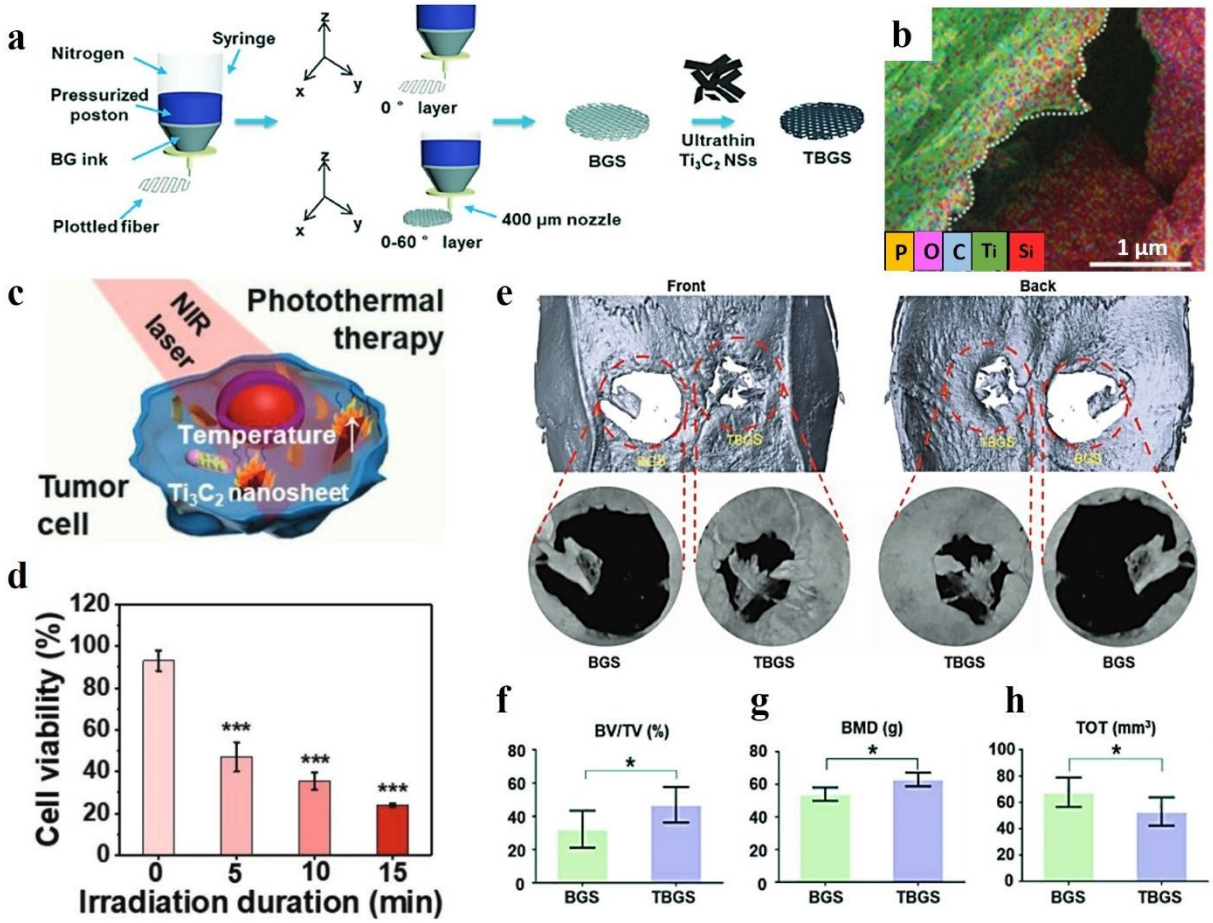


***Figure 5.*** *Characteristics of a 3D-printed $Ti_3C_2$/bioactive glass bone scaffold; (a) schematic design of the synthesis methods, (b) EDS mapping, (c&d) schematic illustration of the photothermal therapy and its outcome, (e) evaluating the 3D reconstruction of the tissue after 24 weeks implantation of the composite tissues, and the value of (f) BV/TV, (g) BMD, and (h) TOT in newborn osseous tissues. Reproduced from reference [17] with permission from Wiley, Copyright 2020.*

MXene films have also illustrated promising features, such as planar structure for regenerating the skin tissue. In a study, a multifunctional crumpled $Ti_3C_2T_x$ MXene-based membrane was designed as a skin tissue scaffold. In this research, various MXene ratios were coated on the polycarbonate membrane using a vacuum filtration technique. According to the results, the mechanical features were enhanced to 30.48% strain, 28.63 MPa tensile strength, and 77.0 dB shielding performance for the membrane containing 70 mg $Ti_3C_2T_x$. This could be attributed to the interfacial interaction between the MXene nanosheets and the 3D fibrous network. So, increasing the MXene ratio up to 70 mg provides more hydrogen bonds and higher mechanical features. The fracture morphology of the MT70 membrane also revealed the tighter attachment of the fibers inside the layer, which could be the reason for attaining superior mechanical properties. Moreover, thermal conductivity was improved by loading more MXene ratio in the membrane.

View Article Online
DOI: 10.1039/D4NH00209A

The through-plane conductivity enhancement refers to the vertical arrangement of the MXene nanosheet on both sides of wrinkles [15].

MXene has also exhibited a fabulous structure as a cardiac patch by mimicking the native tissue regarding its excellent electrical conductivity and topography cues. As an example, Basara et al. [116] designed a 3D-printed $Ti_3C_3T_x$ MXene/PEG composite for cardiac tissue engineering. They confirmed the non-cytotoxicity of the prepared tissue for the human-induced cardiomyocytes. Also, the 3D-printed layer provided a great condition for cell alignment, resulting in the improvement of the synchronous beating and conduction velocity. A similar outcome was also obtained by using $Ti_2C$ cryogel as a conductive bifunctional cardiac patch. The results illustrated the formation of a 3D vessel network after culturing the aortic endothelial cells. Moreover, this membrane represented rapid calcium transient, enhanced cardiac function, and great synchronous heart-like beating. Although the biocompatibility of the MXene-based compositions has been declared by many attempts, long-term biocompatibility assessments seem to be scarce in this era. Accordingly, incorporating systemic toxicity evaluations, immunogenicity assessments, and detailed histopathological analyses of major organs following implantation could substantiate the safety profile of these materials [117].

With the emerging nanotechnology science and the outstanding aptitudes of nanomaterials, they caught a huge interest in tissue regenerating and biomedical applications. These arrays could assist in approaching minimal side effects, passive and active targeting of damaged tissues, time-dependent drug release, and controllable degradation. Considering the vital role of MXene and various electrospun fibers in the progress of tissues, their combination could lead to eliminating their downsides and obtaining a synergetic effect. Accordingly, Awasthi et al. [118] fabricated an electrospun PCL/$Ti_3C_2T_x$ composite and verified its potential for tissue engineering applications. To prepare the specimens, $Ti_3C_2T_x$ with various concentrations of 0.2, 0.5, 1, and 2 wt.% was added into the electrospinning solutions. The electrospinning procedure was carried out using a 12 ml syringe with a nozzle diameter of 0.51 mm under a spinning distance of 15 cm, voltage of 15 kV, and feeding rate of 1 ml/h. **Fig. 6a** shows the TEM illustration of the $Ti_3C_2T_x$-loaded nanofibers. The presence of MXene in the electrospun scaffolds was confirmed by XPS data. The electrospun fibers containing 0.2, 0.5, 1, and 2 wt.% MXene showed average diameters of 0.69, 0.83, 1.32, 1.35, and 1.6 µm, respectively. The increment in the diameter could be due to the presence of interconnected pieces of MXene. The mentioned membranes also exhibited a rise in the contact angle from 100.7 to $37.2^0$ with increasing the MXene concentration, which is fascinating for improving the cell adhesion and proliferation on the surface of scaffolds (see **Fig. 6b&c**). A laboratory biomineralization test was used to evaluate the hydroxyapatite nucleation performance of the generated fibers. The EDS results obtained from the treatment of MXene-reinforced scaffolds with SBF confirmed the sufficient deposition of calcium and phosphorus on the surface of fibers for osseointegration according to the standard values reported for the HA crystals, which could be assigned to the proper wettability of the MXene nanosheets. Biocompatibility was investigated by fibroblast (NIH-3T3) and pre-osteoblast (MC3T3-E1) cells.

View Article Online
DOI: 10.1039/D4NH00209A





According to the results, PCL nanofibers loaded by MXene (up to 0.5 wt.%) represented more biocompatibility compared to the structures embedded with higher MXene ratios. This could be related to incrementing the fibers' diameter, leading to a reduction in protein adsorption, cell viability, and cell adhesion. Therefore, the biological activity of scaffold or bone graft could be boosted resulting from the MXene presence in the electrospun fibers due to its osteogenic properties.

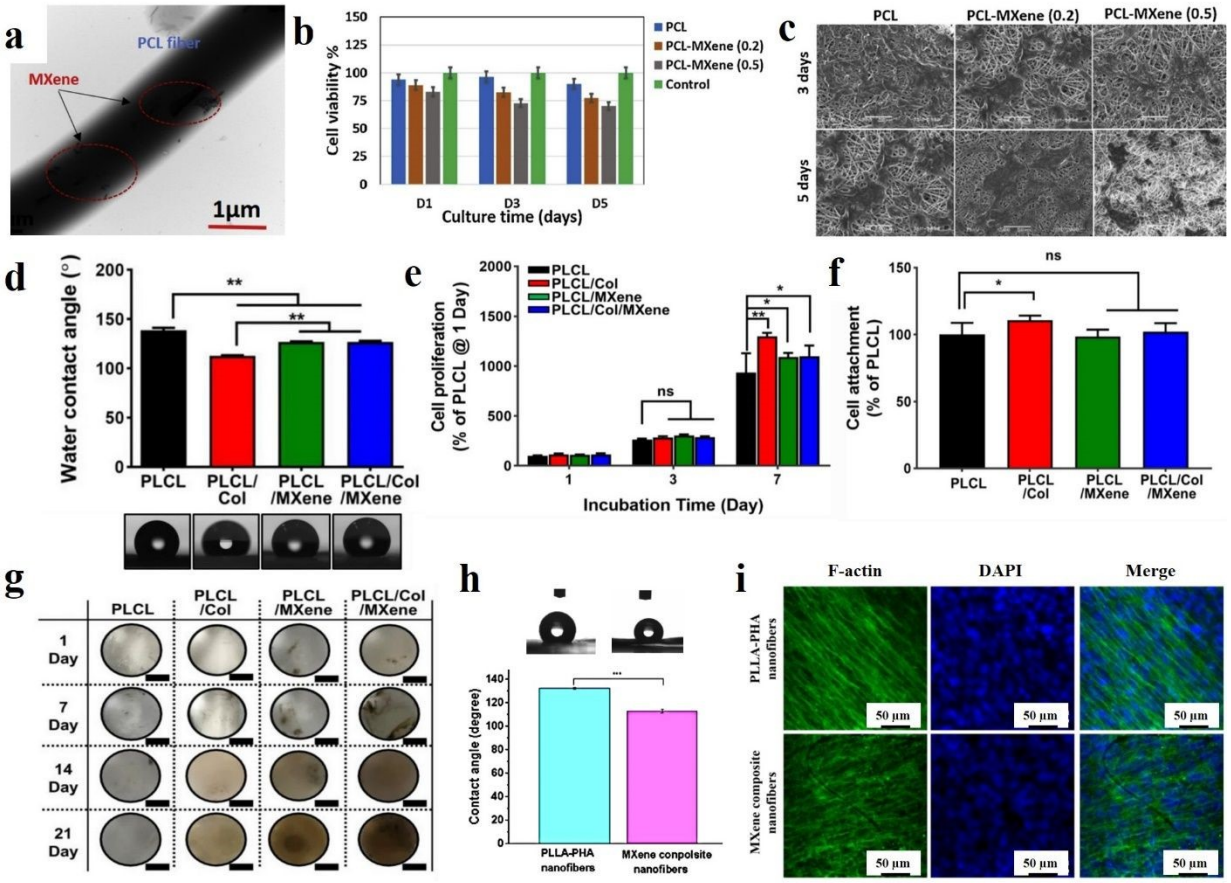


***Figure 6.*** *Various characteristics of the MXene-decorated electrospun scaffolds; (a) TEM, (b) cell viability, and (c) cell attachment of the PCL nanofibers loaded by 0.2 and 0.5% MXene. Reproduced from reference [118] with permission from Elsevier, Copyright 2020. (d) water contact angle, (e) cell proliferation, (f) cell attachment, and (g) digital photographs of von Kossa-stained scaffolds of MXene-loaded PCL/Col nanofibers. Reproduced from reference [119] with permission from Springer, Copyright 2022. (h) water contact angle and (i) fluorescent images of the cultured BMSCs after 5 days of the PLLA-based nanocomposite. Reproduced from reference [23] with permission from the American Chemical Society, Copyright 2020.*

Considering hybrid techniques of film casting and electrospinning, Yan et al. [120] fabricated a highly sensitive bionic MXene-based pressure sensor using the microstructure of the ginkgo leaf. The core deformation part of the sensor possessed microscopic shapes imprinted from the ginkgo

View Article Online
DOI: 10.1039/D4NH00209A



leaves. MXene was sprayed onto a PDMS model film with the ginkgo leaf structure. Also, the PVA nanofibers were synthesized by the electrospinning technique between the MXene component to approach a high-pressure sensitivity of up to 03.46 $kPa^{-1}$. The proposed pressure sensor was durable and displayed a short response time of 99.3 ms, representing the promising potential for application in physiological signal testing and human-computer interaction. Focusing on combining the structures, a triboelectric nanogenerator (TENG) was developed using $Ti_3C_2$ MXene supported by cotton fabric as an electrode layer for self-powered flexible sensors. The MXene was mixed with cellulose nanofibers to create the electrode layer, providing electrical conductivity and negativity, while the cotton fabric boosted strength and flexibility. The generated TENG could produce open-circuit voltage up to 400 V in single-electrode mode and sense the mass of touched steel objects ranging from 2 to 200 g with good repeatability and a linear relationship. The proposed TENG was highly flexible and could be stretched up to 100% of its original length, producing different voltage signals depending on the bending and folding angles. Therefore, the designed structure could be used as a self-powered flexible sensor to monitor various physiological movements of the human body [121].

In 2022, Lee et al. [119] developed nanofibrous matrices of poly(L-lactide-co-ε-caprolactone)/collagen (PLCL/Col) nanofibers loaded by $Ti_3C_2$ nanosheets for bone tissue engineering. First, PLCL (75:25) and Col with concentrations of 5 and 0.5% (w/v) were dissolved in 1, 1, 1, 3, 3, 3-hexafluoroisopropanol. $Ti_3C_2$ was dispersed in deionized water and mixed with PLCL/Col solution to approach the final solution concentration of 400 µg/ml. The electrospinning distance was adjusted to 9 cm. The electrospinning process was carried out with a feeding rate of 0.2 ml/h under a voltage of 16 kV. According to FESEM images, the mean diameter of PLCL, PLCL/Col, PLCL/$Ti_3C_2$, and PLCL/Col/$Ti_3C_2$ nanofibers were 908 ± 68, 449 ± 44, 368 ± 22, and 357 ± 3 nm, respectively. The observed reduction in fiber diameters could be related to the changes in the viscosity of the solutions. Additionally, the surface roughness of the scaffolds also showed a downward trend, possibly due to the formation of finer fibers. As is displayed in **Fig. 6d**, the hydrophilicity of the PLCL scaffold increased with the addition of Col, $Ti_3C_2$, and Col/$Ti_3C_2$ combination. Cell attachment and proliferation of MC3T3-E1 preosteoblasts on the scaffolds were also investigated, implying a significant increase in the cell attachment through the addition of Col into the PLCL matrix compared with that of the PLCL (**Figs. 6e&f**). Meanwhile, there was no significant difference in the cell attachment between the PLCL/$Ti_3C_2$ or PLCL/Col/$Ti_3C_2$ and PLCL. At 7 days of incubation, PLCL/Col and PLCL/Col/$Ti_3C_2$ nanofibrous matrices showed significantly increased cell proliferation, $p < 0.01$ and $p < 0.05$, respectively. The obtained data suggested the synergistic impact of increased initial attachment, as well as hydrophilicity enhancement, in the improvement of cell proliferation. The results of exposure of the scaffolds to cells stained with von Kossa exhibited that the MXene-loaded scaffolds exceptionally increased osteogenesis activity and caused spontaneous differentiation from pre-osteoblasts (see **Fig. 6g**). After cell incubation for 14 days, the mineralized bone nodules appeared on the provided MXene loaded scaffolds, which are stained in a dark-brown color, while the MXene-free membranes did not show any color changes. Therefore, the MXene presence in the structure could lead to stronger

View Article Online
DOI: 10.1039/D4NH00209A

attractive cell interactions, accelerating the $Ca^{2+}$ ions adsorption and so boosting the late-stage osteogenic differentiation.

Huang et al. [23] also fabricated poly-l-lactic acid/Polyhydroxyalkanoates (PLLA/PHA) nanofibers filled with $Ti_3C_2$ for bone tissue engineering. First, 40 mg of $Ti_3C_2$ was added to 4 ml dichloromethane/dimethylformamide (DCM /DMF) and sonicated for 2 hours in an ice bath. Then, 0.16 mg of PLLA and 0.16 g of PHA were introduced into the mixture and stirred for 24h. The electrospinning process was conducted using a 1 ml syringe under a voltage of 15 kV and a feeding rate of 0.6 ml/h. According to the obtained data, fine and homogenous fibers with an average diameter of 850 nm ranging from 600 nm to 1.5 µm. were obtained. The XPS data revealed the creation of a large number of -OH and -O- terminal groups on the nanofibers' surfaces. The contact angle of the electrospun composites decreased from 132.27 to 112.76° after the incorporation of $Ti_3C_2$ into the PLLA/PHA nanofibers, resulting from the MXene functional groups (see **Fig. 6h**). Bone marrow-derived mesenchymal stem cells (BMSCs) were seeded on the scaffolds for 1, 3, 7, and 14 days. The results confirmed the cell adhesion enhancement on the MXene-loaded scaffolds after day 1, which could be attributed to the rise in the hydrophilicity ratio. On day 3, a similar trend was observed in the cell adhesion between the samples with and without MXene nanosheets. Meanwhile, it was again enhanced in the filled membrane after day 7, which could be linked with the formation of a desirable microenvironment for cell adhesion and proliferation. SEM images of cell culture on the scaffolds showed the spreading of the BMSCs cells along the nanofibrous pattern and the formation of a fiber-cell network (see **Fig. 6i**). The results of the PCR test displayed that the scaffolds reinforced with MXene had better osteogenesis functions than the filler-free scaffold after 14 days.

In 2023, Fu et al. [25] produced $Ti_3C_2T_x$/PVDF nanofibers through a standard electrospinning process for bone scaffolds. PVDF was first dissolved in a mixture of N, N-dimethylformamide/ acetone (3:2), and the solution with a concentration of 20 wt./v% was obtained after 2h stirring at 50°C. Then, 0.2, 1, and 5% $Ti_3C_2T_x$ were sonicated in the obtained polymer solution at 4°C for 30 min, followed by a stirring step of 8h at ambient temperature. The prepared solution was transferred to a syringe with a 20-gauge nozzle and electrospun with a feeding rate of 0.8 ml/min under a voltage of 13 kV and a spinning distance of 15 cm. The filler-free PVDF, as well as the loaded samples with 0.2, 1, and 5% $Ti_3C_2T_x$, represented average diameters of 854.6 ± 300.4, 803.4 ± 245.9, 648.9 ± 215.5, and 538.8 ± 171.1 nm, respectively. The destruction examination confirmed the high stability of the provided scaffold structures and corroborated the role of the PVDF shell in hindering MXene oxidation. According to the results, the PVDF scaffold is a hydrophobic layer (116.47 ± 0.99°), and its contact angle and hydrophobicity was increased to 125.45 ± 1.88, 123.72 ± 2.20, and 124.85 ± 1.87° by adding 0.2, 1, and 5 wt % MXene, respectively. These results are in contrast with previous studies, which can be stated that the PVDF leaf layer prevents the contact of MXene with water droplets, and it is also speculated that the addition of MXene increases the hydrophobicity of the structure due to the reduction of the surface free energy and the increase of the pore structure. The pure PVDF scaffold showed a tensile strength of 0.94

View Article Online
DOI: 10.1039/D4NH00209A

± 0.12 MPa and Young's modulus of 0.82 ± 0.22 MPa. Embedding up to 1% MXene into the PVDF structure caused an increase in the tensile strength (4.49 ± 0.33 MPa), while loading 5% led to a reduction in the tensile value (1.52 ± 0.29 MPa) (see **Figs. 7a&b**). Accordingly, a small amount of MXene could raise the modulus, possibly due to the strong interaction force between PVDF molecular chains and MXene functional groups. However, exceeding a specific loading ratio led to filler agglomeration and so a reduction in the scaffold modulus.

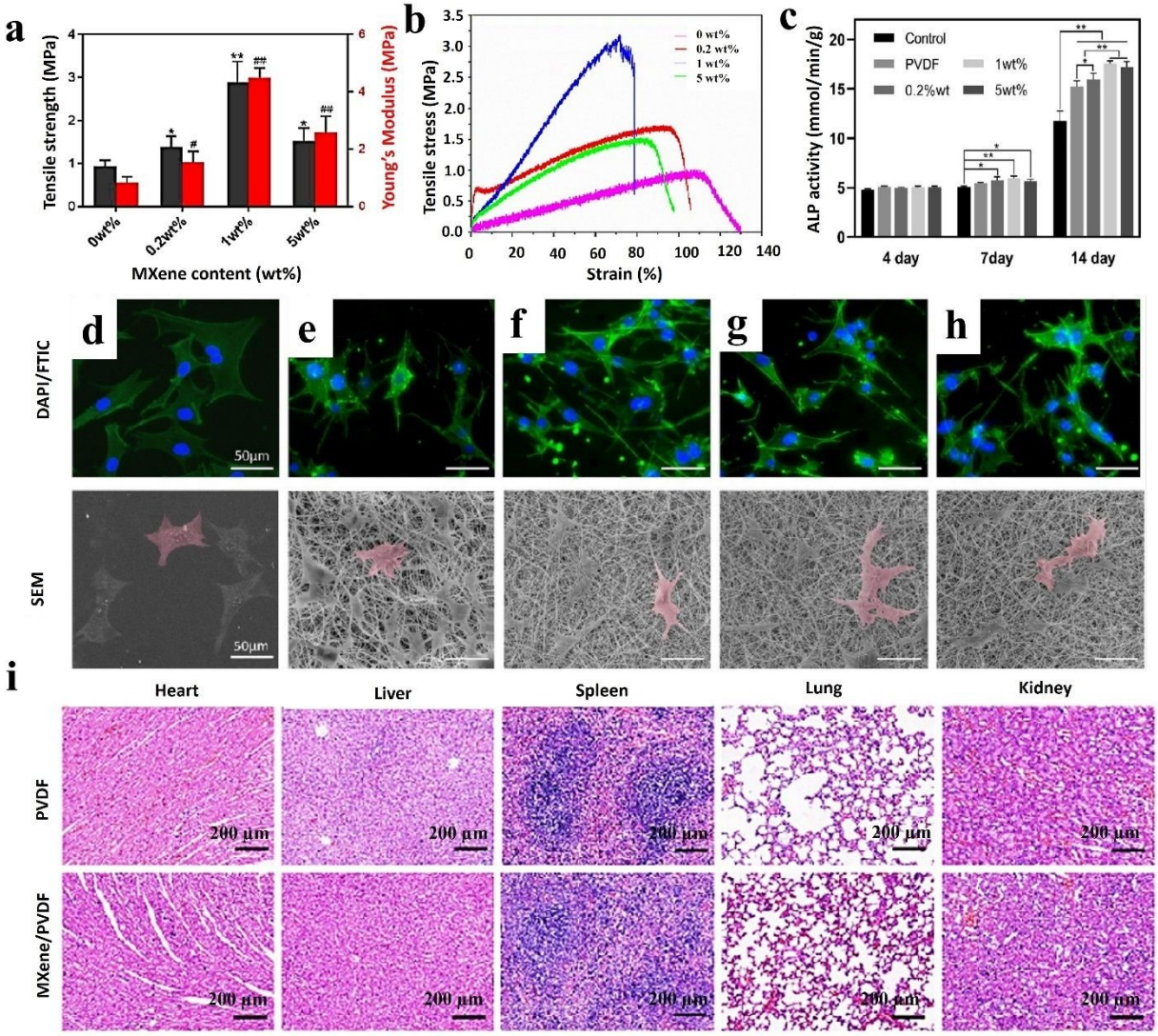


***Figure** 7. Features of the MXene/PVDF nanofibrous bone scaffolds; (a&b) mechanical properties, (c) ALP activity, morphology, and adhesion of MC3T3-E1 cells on (d) glass, (e) pristine PVDF, (f) 0.2 wt % MXene/PVDF, (g) 1 wt. % MXene/PVDF, and (h) 5 wt % MXene/PVDF, and (i) H&E staining images after employing different treatments for 8 weeks in various organs, including heart, liver, spleen, lung, and kidney stained with hematoxylin−eosin. Reproduced from reference [25] with permission from the American Chemical Society, Copyright 2023.*

View Article Online
DOI: 10.1039/D4NH00209A





Staining of dead cells was performed by inoculating MC3T3-E1 on the scaffolds for 24h, showing acceptable cell viability by incorporating up to 1% MXene while increasing the dead cells through loading 5% MXene (see **Figs. 7c-h**). The fluorescence microscope proved the spreading of the MC3T3-E1 cells after 3 days on the surface of the scaffolds, which could be attributed to the 3D topographical structure of the electrospun fibers. To investigate the effective substances on the biological behavior of cells, a scratch test was conducted, showing similar migration of cells into the gaps in all samples after 24 and 48h. This phenomenon confirms the hypothesis of MXene placement in the PVDF shell, which does not affect the external cellular environment. The cell viability assay confirmed the suitability of the scaffolds for cell growth. The results of cell culture after 4 days were the same in all samples, but after 7 days scaffolds, containing 0.2% and 1% MXene showed the highest cell viability. This could be attributed to the difference in surface potential and topography of fibers, resulting from loading various amounts of MXene. The ALP activity of cells after 14 days in samples containing MXene was higher than that in the pristine PVDF, linking with the increase in surface potential and the fibers' topography. To evaluate the osteogenic activity of camels, the relative expression of the MC3T3-E1 bone gene, including OCN, OPN, ALP, Runx2, and Col I, was cultured and investigated. Accordingly, incorporating 1% MXene mainly regulates the expression level of osteogenic genes in both early and late periods, representing the great ability to improve osteogenic differentiation with a potential of 69.34 ± 2.64 mV.

Finally, animal tests exhibited the appearance of normal branched muscle fibers in heart tissue, radially scattered cells in liver tissue, ideal splenic nodules in the spleen, proper alveoli and epithelial lining of bronchioles in lung tissue, and glomeruli and tubules for 8 weeks (see **Fig. 7i**). No significant difference was observed in the pathological results of the PVDF and PDF/MXene scaffolds on different organs, which indicates their outstanding biocompatibility. Also, new tissues were formed at the site of the bone defect after 4 and 8 weeks of treatment. The surface potential of the scaffold enhanced the differentiation of bone-forming cells and the absorption of osteogenic cells on the surface of the scaffold, allowing the bone defect to be filled after 8 weeks. Other recent attempts toward integrating the nanofibers via embedding MXene nanosheets toward approaching efficient tissues, as well as versatile healthcare devices, are summarized in Table 1.

***Table 1.*** *MXene-loaded electrospun fibers applicable as various biomedical devices and tissue engineering membranes.*

| Material contents | Application | Mechanism and Results | Ref. |
|---|---|---|---|
| MXene/Amoxicillin/PVA | Antimicrobial and photothermal platform for wound infection | -PVA matrix could control the Amoxicillin release.<br>-MXene presented local Hyperthermia due to transforming the NIR laser into heat in battling bacterial infection. | Xu et al. [122] |

View Article Online
DOI: 10.1039/D4NH00209A



| | | | |
|---|---|---|---|
| | | -The nanomembrane exhibited an antibacterial and accelerated wound healing capacity in the in vivo and in vitro models. | |
| **TiC/zeolite imidazole framework-8 (MZ-8)/PLA** | Wound healing | -MZ-8 could show hyperthermia PPT activity with a bactericidal rate of more than 99.0% and remarkable antitumor efficiency relying on photodynamic/photothermal therapy.<br>-MXene/zeolite/PLA could boost infected wound healing without any bacteria resistance. | Zhang et al. [123] |
| $Ti_3C_2T_x$/chitosan | Antibacterial wound dressing | -In vitro, antibacterial activity was depicted via crosslinked chitosan nanofibers integrated with MXene.<br>-Direct bacterial membrane destruction was observed by contacting and penetrating bacteria in MXene flakes, with a 95% to 62% reduction in colony-forming units.<br>-The features were synergized with intrinsic chitosan antimicrobial activity. | Mayerberger et al. [124] |
| $Ti_3AlC_2$ MAX phase/PLA | Curcumin delivery system with antibacterial behavior | -PLA electrospun membranes decorated with MAX phase exhibited significantly higher toughness than the plasticized PLA membrane with low cytotoxicity, supporting the proliferation of mouse fibroblast L929 cells, as well as higher antibacterial properties against E. coli and S. aureus.<br>-Due to the curcumin diffusion from the polymer fibers and the MAX phase surface contributing to the overall increased curcumin adsorption and release sites, 7-day curcumin release was increased from 45 to 67%. | Krasian et al. [125] |
| PVA/ $Ti_3C_2T_x$/ Molybdenum Diselenide **(**$MoSe_2$)/ polyethylene terephthalate | Human skin moisture/Energy harvesting sensor | -Self-powered sensing device was fabricated by PVA/MXene nanolayer and integrated with a single layer of $MoSe_2$ to decipher humidity by commuting mechanical energy to electric energy.<br>-The excellent metallic conductivity and hydrophilicity of PVA/MXene, concomitant with the piezoelectric properties of $MoSe_2$ generated the flexible, fast response humidity sensor (0.9/6.3 s, about 40-fold higher than pure MXene). | Wang et al. [126] |
| $Ti_3C_2T_x$/PVDF | Aptasensors | -The designed nanocomposite detected secondary fungal metabolite mycotoxin due to their electroactive sites and covalent biofunctionalization of the redox probe with aptamer.<br>-The designed sensor was useful for OTA trace determination in the food safety analysis in the concentration range from 1 $fg.mL^{-1}$ to 1 $ng.mL^{-1}$. | Al-Dhahebi et al. [127] |
| $Ti_3C_2T_x$/dopamine/polyurethane | Wearable sensor | -The inclusion of thermoplastic polyurethane in the composition offered enhanced flexibility and breathability. | Zhang et al. [128] |

View Article Online
DOI: 10.1039/D4NH00209A



| | | | |
|---|---|---|---|
| | | -The presence of a poly-dopamine coating facilitated adhesion between MXene and thermoplastic polyurethane.<br>-The incorporation of MXene resulted in strain-sensing capabilities and effective electromagnetic interference shielding performance.<br>-The strain sensor design exhibited remarkable sensing functionality, demonstrating an exceptional recognition threshold. | |
| $Ti_3C_2T_x$/PCL | Neurite regeneration and angiogenesis | -The PCL layer was covered with MXene, and figured out the excellent cell adhesion and biocompatibility during cell culturing.<br>-MXene-PCL composite for nerve guidance conduits showed similar results with the autograft in angiogenesis, electrophysiological examination, and nerve regeneration morphology in both in vivo and in vitro studies. | Nan et al. [129] |
| $Ti_3C_2T_x$/PLA | Nerve guidance conduits | -The functionalized layer exhibited biocompatibility and non-toxicity through the Cell culturing test and gram-positive bacterial adhesion assay.<br>-MXene directly influences cellular membranes and damages the cell morphology.<br>-Fabulous electroconductivity properties were confirmed with an electrical conductivity assay due to the MXene involved in PLA membranes. | Kyrylenko et al. [130] |
| $Ti_3C_2T_x$/PCL | Tissue engineering | -The effect of MXene layer thickness was evaluated, showing the most appropriate results of cell attachment, adhesion, and proliferation, as well as antibacterial behavior through repeating the immersing process 2 and 3 times.<br>-These samples exhibited samples illustrated the least bacteria adhesion due to the inhibitory effect of the MXene thin layers on the membrane surface through physical damaging of the cell walls. | Diedkova et al. [131] |
| $Ti_3C_2T_x$/PLGA | Nerve tissue regeneration | -The formation of a more brittle structure via exceeding the MXene ratio from 0.1 g.<br>- Antibacterial property of the produced scaffolds against E. coli, S. aureus, and C. albicans, due to high hydrophilicity and the bacteria absorption by surface anions of MXene nanosheets.<br>- The results of the biocompatibility test were performed with the cultivation of Schwann cells on the scaffolds, illustrating the cell survival on the scaffolds containing 0.3 and 0.6 MXene, which is due to the increased hydrophilicity and conductivity. | Zhang et al. [132] |

View Article Online
DOI: 10.1039/D4NH00209A



Overall, flexible nanofibrous networks with tunable morphological features, as well as mechanical strength, could be feasibly synthesized through the electrospinning method. The highly porous structure of the electrospun fibers with interconnected pores could offer favorable features for biomedical targets and mimic the native extracellular matrix, integrating cell adhesion, growth, and proliferation in various organs. Although electrospun nanofibers embedded with MXene nanostructures have showcased promising configurations for biomedical targets, a lack of long-term evaluation is sensed in the performed analysis. As an example, mechanical properties are considered as one of the main features, requiring to be optimized considering each application. For example, in the context of tissue engineering, the designed structure must possess mechanical properties that are appropriate for the desired vein. Failure to do so may result in the degradation of the original tissue or the collapse of the new structure when subjected to load [2]. The analysis of the mechanical stability in bodily fluids or under cyclic loadings mimicking bodily movements could provide valuable insights into their long-term durability in biomedical applications. To assess the mechanical properties of the designed structures, it is recommended that they be tested under conditions that are similar to those found in vivo. For instance, the samples should be immersed in a buffer solution or subjected to cell culture. Furthermore, it is advisable to test the samples under both unidirectional and multidirectional conditions, depending on the intended application. Consequently, the mechanical properties of the designed structures must be carefully evaluated to ensure that they are fit for purpose [133].

Moreover, long-term cytotoxicity analysis is assumed to be a critical issue in biomedical applications. Therefore, verifying the long-term compatibility and non-toxicity of materials is of utmost importance. While various case studies have investigated the acute toxicological effects of MXene-based compositions in vitro and in vivo, few studies have been dedicated to highlighting its long-term toxicology behavior [134]. To address this, in vitro studies utilizing long-term cell cultures and monthly observations are recommended. Additionally, the degradation of samples under physiological conditions should be investigated over an extended period to ascertain if any toxic substances are released or if the pH and other environmental factors are altered over time [2, 133].

## Conclusion and perspectives

As a very promising emerging material, the MXene family has shown outstanding features for a wide range of applications. Several inherent MXene characteristics, including frequent functional groups on the surface, biocompatibility, large surface-to-volume ratio, physiochemical properties, and many more, have caused a plethora of benefits for biomedical usages and tissue engineering targets. Among various MXene-loaded compositions, the electrospun fibrous architectures have represented promising features resulting from the large surface area, highly porous networks, tiny and interconnected pores, etc. The integration of electrospun fibers with MXene nanosheets could boost hydrophilicity and enhance dimensional and mechanical stability. Additionally, biocompatibility, antibacterial activity, as well as cell adhesion, growth, and proliferation could be integrated into these platforms, leading to approaching ideal bone, nerve, skin, and heart tissues.

View Article Online
DOI: 10.1039/D4NH00209A

Accordingly, the electrospun tissues embedded with MXene nanosheets could alleviate the challenges faced by individual components, benefiting from their synergetic effects.

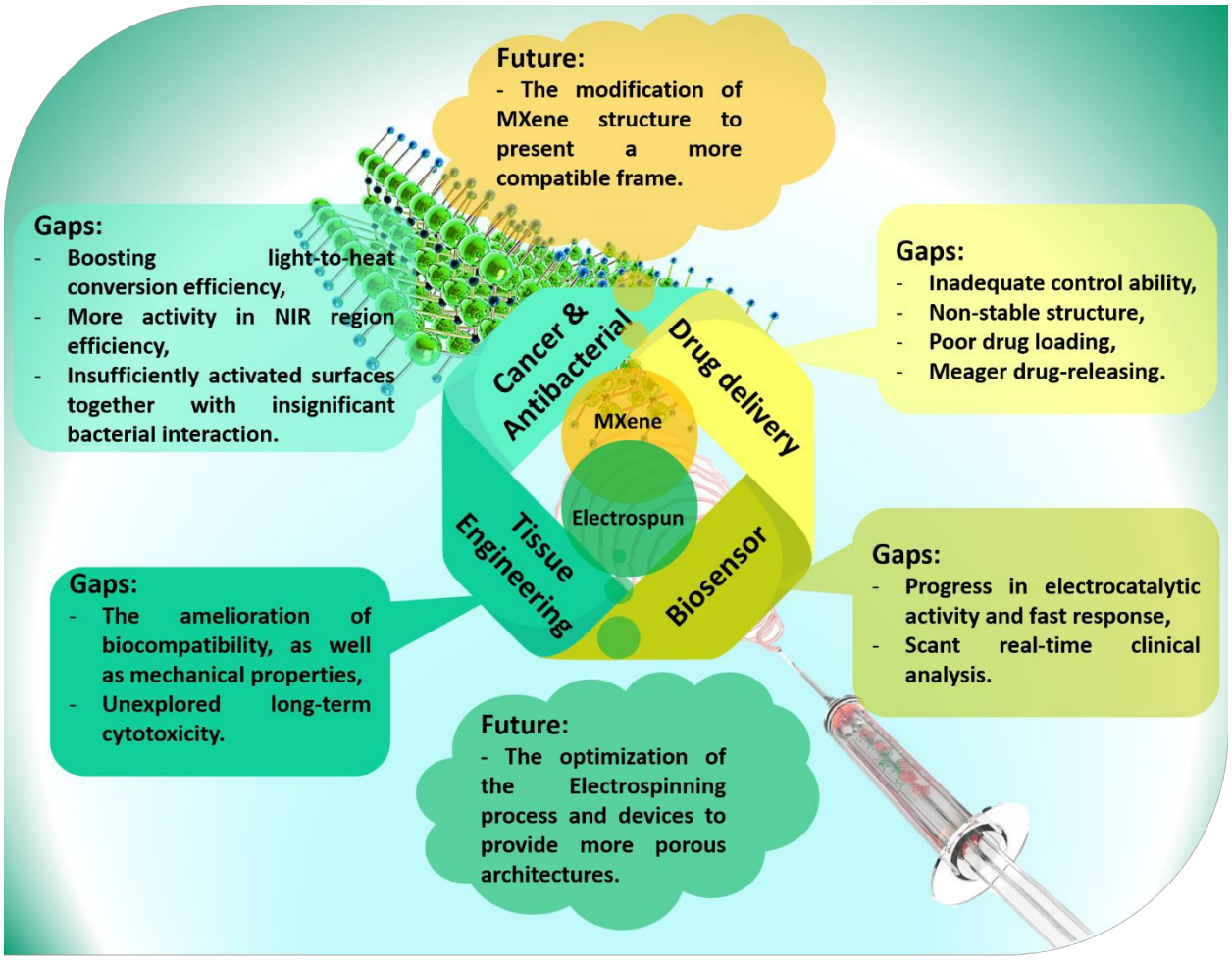


***Figure 8.*** *Prospects for the future and gaps in biomedical applications; the developed path of MXene and electrospun frameworks.*

Despite the great consequences observed for the MXene-loaded nanocomposites, few researches have been conducted in this era, leading to several remaining challenges (**Fig. 8**). First, in competition with the present strategies, synthesis modification, surface functionalizing, and morphology altering are proposed to be investigated more, since they could be influential on the cytotoxicity and biocompatibility. Also, MXene is nonstable in the atmosphere and physiological environments. The employed synthesis method should be progressed to achieve an eco-friendly, long-term stable, adjustable, and cost-effective technique with least-hazard byproducts. In addition, the biological behavior of the MXene-loaded materials should be focused more to further evaluate long-term toxicity, the reaction of MXene with cells, drugs, blood, and organs, biodegradability, biosafety, and histopathological properties. It is important to consider that the use of toxic and

View Article Online
DOI: 10.1039/D4NH00209A

corrosive liquids in the synthesis of MXene could result in negative effects. Also, most of the research in this era is focused on the use and development of titanium carbide-based additives, while the MXene family is very broad, and the lack of suitable explorations is deeply felt. This route could also be continued through the design and analysis of the MXene combination or coating with other organic and inorganic compounds in the electrospun configurations. It is worthwhile to manipulate the electrospinning fabrication procedure to obtain more monotonous fibrous networks comprising tunable pore sizes and porosity rates.

In the biomedical path, the physiological, biological, and mechanical features of nanofibrous membranes play a critical role in the final success of designed architectures. In this regard, it is proposed to amend the surface of nanofibrous layers through direct electrospinning of polymers with organic-based components, as well as applying surface modification techniques, such as plasma treatment, surface polishing, and others. The electrospun membranes could be integrated with other MXene-loaded arrays, such as hydrogel, 3D-printed, or electro-written layers. Moreover, in vitro and in vivo analyses are suggested to be carried out on various tissues generated with the MXene and MXene derivatives-loaded materials. Furthermore, comprehensive studies along with the simulation and modeling are offered for the prediction of MXene-loaded nanofibrous tissues' behavior without the need for animal studies. However, it is also understandable that most studies are currently limited to lab scale, which can create skepticism towards MXene-embedded electrospun structures. Accordingly, a need is recognized for more comprehensive studies in order to alleviate these concerns and ensure a safer and more sustainable approach. MXene-embedded electrospun structures have the potential to revolutionize various fields by offering unique combinations of properties and functionalities. Ongoing research and development efforts will further advance this material system and unlock its full potential for next-generation technologies.

## Funding.

The authors acknowledge the Foundation of China (Grant No.51702204), the Natural Science Foundation of Shaanxi Province (Grant No. 2017JQ2043), Xianyang Science and Technology Research Project of China (Grant No. 2021ZDYF-GY-0040), and Xianyang City Qinchuangyuan Science and Technology Innovation Special Project (Grant No. L2022-QCYZX-GY-006).

## Contributions.

X. Li: Collecting data, Writing the paper, and Validating data.

S. Wang: Collecting data, Writing the paper, and Designing the figures.

M. Zheng: Writing the paper and Approved data

Z. Ma: Writing the paper and Designing the figures

Y. Chen: Collecting Data and Writing the paper

L. Deng: Designing the project and Collecting data

W. Xu: Writing the paper, Approving data, and Designing figures

G. Fan: Administrating the paper and Revising the paper

View Article Online
DOI: 10.1039/D4NH00209A

S. Khademolqorani: Writing and revising the paper and Designing the figures

SN. Banitaba: Writing and revising the paper and Designing the figures

AI. Osman: Administrating the paper and Revising the paper

# References.

[1] K. Ghosal, C. Agatemor, Z. Špitálsky, S. Thomas, and E. Kny, "Electrospinning tissue engineering and wound dressing scaffolds from polymer-titanium dioxide nanocomposites," *Chemical Engineering Journal,* vol. 358, pp. 1262-1278, 2019.

[2] S. Khademolqorani, H. Tavanai, I. S. Chronakis, A. Boisen, and F. Ajalloueian, "The determinant role of fabrication technique in final characteristics of scaffolds for tissue engineering applications: A focus on silk fibroin-based scaffolds," *Materials Science and Engineering: C,* vol. 122, p. 111867, 2021.

[3] M. Nasari, N. Poursharifi, A. Fakhrali, S. N. Banitaba, S. Mohammadi, and D. Semnani, "Fabrication of novel PCL/PGS fibrous scaffold containing HA and GO through simultaneous electrospinning-electrospray technique," *International Journal of Polymeric Materials and Polymeric Biomaterials,* pp. 1-17, 2022.

[4] S. Khademolqorani and S. N. Banitaba, "Application of electrosprayed nanoparticles as targeted drug delivery systems: A mini review," *Journal of Applied Sciences and Nanotechnology,* vol. 2, no. 2, pp. 1-7, 2022.

[5] M. Rahmati *et al.*, "Electrospinning for tissue engineering applications," *Progress in Materials Science,* vol. 117, p. 100721, 2021.

[6] X. Xie *et al.*, "Electrospinning nanofiber scaffolds for soft and hard tissue regeneration," *Journal of Materials Science & Technology,* vol. 59, pp. 243-261, 2020.

[7] A. P. Rickel, X. Deng, D. Engebretson, and Z. Hong, "Electrospun nanofiber scaffold for vascular tissue engineering," *Materials Science and Engineering: C,* vol. 129, p. 112373, 2021.

[8] E. R. Ghomi *et al.*, "Advances in electrospinning of aligned nanofiber scaffolds used for wound dressings," *Current Opinion in Biomedical Engineering,* p. 100393, 2022.

[9] S. N. Banitaba *et al.*, "Biopolymer-based electrospun fibers in electrochemical devices: versatile platform for energy, environment, and health monitoring," *Materials Horizons,* vol. 9, no. 12, pp. 2914-2948, 2022.

[10] S. Khademolqorani, S. N. Banitaba, S. Azizi, and M. Kouhi, "Chapter 9 - Gellan gum–based nanocomposite hydrogels," in *Application of Gellan Gum as a Biomedical Polymer*, A. K. Nayak and M. S. Hasnain Eds.: Academic Press, 2024, pp. 171-197.

[11] S. Nagam Hanumantharao and S. Rao, "Multi-functional electrospun nanofibers from polymer blends for scaffold tissue engineering," *Fibers,* vol. 7, no. 7, p. 66, 2019.

[12] R. A. Surmenev *et al.*, "Electrospun composites of poly-3-hydroxybutyrate reinforced with conductive fillers for in vivo bone regeneration," *Open Ceramics,* vol. 9, p. 100237, 2022.

[13] S. Khademolqorani, A. Zeinal Hamadani, and H. Tavanai, "Response Surface Modelling of Electrosprayed Polyacrylonitrile Nanoparticle Size," *Journal of Nanoparticles,* vol. 2014, p. 146218, 2014/08/10 2014, doi: 10.1155/2014/146218.

[14] L. Yang *et al.*, "Wearable pressure sensors based on MXene/tissue papers for wireless human health monitoring," *ACS Applied Materials & Interfaces,* vol. 13, no. 50, pp. 60531-60543, 2021.

View Article Online
DOI: 10.1039/D4NH00209A



[15] R. Ding *et al.*, "Skin inspired multifunctional crumpled Ti3C2Tx MXene/Tissue composite film," *Composites Part A: Applied Science and Manufacturing,* vol. 158, p. 106967, 2022/07/01/ 2022, doi: https://doi.org/10.1016/j.compositesa.2022.106967.

[16] S. Iravani and R. S. Varma, "MXenes and MXene-based materials for tissue engineering and regenerative medicine: Recent advances," *Materials Advances,* vol. 2, no. 9, pp. 2906-2917, 2021.

[17] S. Pan *et al.*, "2D MXene-integrated 3D-printing scaffolds for augmented osteosarcoma phototherapy and accelerated tissue reconstruction," *Advanced Science,* vol. 7, no. 2, p. 1901511, 2020.

[18] C. Yang, Y. Luo, H. Lin, M. Ge, J. Shi, and X. Zhang, "Niobium carbide MXene augmented medical implant elicits bacterial infection elimination and tissue regeneration," *ACS nano,* vol. 15, no. 1, pp. 1086-1099, 2020.

[19] J. Zhang, Y. Fu, and A. Mo, "Multilayered titanium carbide MXene film for guided bone regeneration," *International journal of nanomedicine,* pp. 10091-10103, 2019.

[20] J. Yin *et al.*, "MXene-based hydrogels endow polyetheretherketone with effective osteogenicity and combined treatment of osteosarcoma and bacterial infection," *ACS applied materials & interfaces,* vol. 12, no. 41, pp. 45891-45903, 2020.

[21] Q. Yang *et al.*, "Engineering 2D mesoporous Silica@ MXene-integrated 3D-printing scaffolds for combinatory osteosarcoma therapy and NO-augmented bone regeneration," *Small,* vol. 16, no. 14, p. 1906814, 2020.

[22] G. Ye *et al.*, "Mussel-inspired conductive Ti2C-cryogel promotes functional maturation of cardiomyocytes and enhances repair of myocardial infarction," *Theranostics,* vol. 10, no. 5, p. 2047, 2020.

[23] R. Huang *et al.*, "MXene composite nanofibers for cell culture and tissue engineering," *ACS Applied Bio Materials,* vol. 3, no. 4, pp. 2125-2131, 2020.

[24] M. Naguib *et al.*, "Two-dimensional nanocrystals produced by exfoliation of Ti3AlC2," *Advanced materials,* vol. 23, no. 37, pp. 4248-4253, 2011.

[25] Y. Fu *et al.*, "MXene-Functionalized Ferroelectric Nanocomposite Membranes with Modulating Surface Potential Enhance Bone Regeneration," *ACS Biomaterials Science & Engineering,* 2023.

[26] M. Rafiq *et al.*, "Recent progress in MXenes incorporated into electrospun nanofibers for biomedical application: Study focusing from 2017 to 2022," *Chinese Chemical Letters,* vol. 34, no. 7, p. 108463, 2023/07/01/ 2023, doi: https://doi.org/10.1016/j.cclet.2023.108463.

[27] B. Pant, M. Park, and A. A. Kim, "MXene-Embedded Electrospun Polymeric Nanofibers for Biomedical Applications: Recent Advances," *Micromachines,* vol. 14, no. 7, p. 1477, 2023.

[28] Y. Feng *et al.*, "The collagen-based scaffolds for bone regeneration: A journey through electrospun composites integrated with organic and inorganic additives," *Processes,* vol. 11, no. 7, p. 2105, 2023.

[29] S. N. Banitaba, A. A. Gharehaghaji, and A. A. A. Jeddi, "Fabrication and characterization of hollow electrospun PLA structure through a modified electrospinning method applicable as vascular graft," *Bulletin of Materials Science,* vol. 44, pp. 1-7, 2021.

[30] J. Xue, T. Wu, Y. Dai, and Y. Xia, "Electrospinning and electrospun nanofibers: Methods, materials, and applications," *Chemical reviews,* vol. 119, no. 8, pp. 5298-5415, 2019.

[31] M. Z. A. Zulkifli, D. Nordin, N. Shaari, and S. K. Kamarudin, "Overview of Electrospinning for Tissue Engineering Applications," *Polymers,* vol. 15, no. 11, p. 2418, 2023.

[32] D. Ji *et al.*, "Electrospinning of nanofibres," *Nature Reviews Methods Primers,* vol. 4, no. 1, p. 1, 2024.

[33] R. Jalili, S. A. A. HOSSEINI, and M. Morshed, "The effects of operating parameters on the morphology of electrospun polyacrilonitrile nanofibres," 2005.

View Article Online
DOI: 10.1039/D4NH00209A



[34] K. Matabola and R. Moutloali, "The influence of electrospinning parameters on the morphology and diameter of poly (vinyledene fluoride) nanofibers-effect of sodium chloride," *Journal of Materials Science,* vol. 48, pp. 5475-5482, 2013.

[35] H. Liu, S. Vijayavenkataraman, D. Wang, L. Jing, J. Sun, and K. He, "Influence of electrohydrodynamic jetting parameters on the morphology of PCL scaffolds," *International Journal of Bioprinting,* vol. 3, no. 1, 2017.

[36] A. Jabur, L. Abbas, and S. Muhi Aldain, "Effects of ambient temperature and needle to collector distance on PVA nanofibers diameter obtained from electrospinning technique," *Engineering and Technology Journal,* vol. 35, no. 4A, pp. 340-347, 2017.

[37] S. Shen, Y. Wu, Y. Liu, and D. Wu, "High drug-loading nanomedicines: progress, current status, and prospects," *International journal of nanomedicine,* pp. 4085-4109, 2017.

[38] H. Laroui *et al.*, "Nanomedicine in GI," *American Journal of Physiology-Gastrointestinal and Liver Physiology,* vol. 300, no. 3, pp. G371-G383, 2011.

[39] Z. Chen, M. Guan, Y. Bian, and X. Yin, "Multifunctional Electrospun Nanofibers for Biosensing and Biomedical Engineering Applications," *Biosensors,* vol. 14, no. 1, p. 13, 2023.

[40] S. Gungordu Er, A. Kelly, S. B. W. Jayasuriya, and M. Edirisinghe, "Nanofiber based on electrically conductive materials for biosensor applications," *Biomedical Materials & Devices,* vol. 1, no. 2, pp. 664-679, 2023.

[41] S. N. Banitaba *et al.*, "Recent progress of bio-based smart wearable sensors for healthcare applications," *Materials Today Electronics,* vol. 5, p. 100055, 2023.

[42] S. N. Banitaba, A. A. Q. Ahmed, M.-R. Norouzi, and S. Khademolqorani, "Biomedical applications of non-layered 2DMs," 2023.

[43] J. T. McCann, M. Marquez, and Y. Xia, "Highly Porous Fibers by Electrospinning into a Cryogenic Liquid," *Journal of the American Chemical Society,* vol. 128, no. 5, pp. 1436-1437, 2006/02/01 2006, doi: 10.1021/ja056810y.

[44] C. Huang and N. L. Thomas, "Fabricating porous poly(lactic acid) fibres via electrospinning," *European Polymer Journal,* vol. 99, pp. 464-476, 2018/02/01/ 2018, doi: https://doi.org/10.1016/j.eurpolymj.2017.12.025.

[45] N. E. Zander, J. A. Orlicki, A. M. Rawlett, and T. P. Beebe Jr, "Electrospun polycaprolactone scaffolds with tailored porosity using two approaches for enhanced cellular infiltration," *Journal of Materials Science: Materials in Medicine,* vol. 24, no. 1, pp. 179-187, 2013.

[46] P. Fomby *et al.*, "A review of key challenges of electropsun scaffolds for tissue-engineering applications," *Ann. Am. Thorac. Soc,* vol. 12, pp. 181-204, 2010.

[47] L. Yang *et al.*, "Electrospun silk fibroin/fibrin vascular scaffold with superior mechanical properties and biocompatibility for applications in tissue engineering," *Scientific Reports,* vol. 14, no. 1, p. 3942, 2024/02/16 2024, doi: 10.1038/s41598-024-54638-0.

[48] H. Lee *et al.*, "Enhancement of mechanical properties of polymeric nanofibers by controlling crystallization behavior using a simple freezing/thawing process," *RSC Advances,* 10.1039/C7RA06545K vol. 7, no. 69, pp. 43994-44000, 2017, doi: 10.1039/C7RA06545K.

[49] D. Xu, Z. Li, Z. Deng, X. Nie, Y. Pan, and G. Cheng, "Degradation profiles of the poly (ε-caprolactone)/silk fibroin electrospinning membranes and their potential applications in tissue engineering," *International Journal of Biological Macromolecules,* p. 131124, 2024.

[50] H. Budharaju *et al.*, "Carboxymethyl cellulose-agarose hydrogel in poly (3-hydroxybutyrate-co-3-hydroxyvalerate) nanofibers: A novel tissue engineered skin graft," *International Journal of Biological Macromolecules,* p. 130565, 2024.

[51] Y. H. Jeong, M. Kwon, S. Shin, J. Lee, and K. S. Kim, "Biomedical Applications of CNT-Based Fibers," *Biosensors,* vol. 14, no. 3, p. 137, 2024. [Online]. Available: https://www.mdpi.com/2079-6374/14/3/137.

View Article Online
DOI: 10.1039/D4NH00209A

[52] N. Nazeri, M. A. Derakhshan, R. Faridi-Majidi, and H. Ghanbari, "Novel electro-conductive nanocomposites based on electrospun PLGA/CNT for biomedical applications," *Journal of Materials Science: Materials in Medicine,* vol. 29, pp. 1-9, 2018.
[53] M. C. Barbosa *et al.*, "Production of rGO-Based Electrospinning Nanocomposites Incorporated in Recycled PET as an Alternative Dry Electrode," *Polymers,* vol. 14, no. 20, p. 4288, 2022. [Online]. Available: https://www.mdpi.com/2073-4360/14/20/4288.
[54] Z. Liu *et al.*, "Graphene-based materials prepared by supercritical fluid technology and its application in energy storage," *The Journal of Supercritical Fluids,* vol. 188, p. 105672, 2022.
[55] A. Ivanoska-Dacikj *et al.*, "Electrospun PEO/rGO Scaffolds: The Influence of the Concentration of rGO on Overall Properties and Cytotoxicity," *International Journal of Molecular Sciences,* vol. 23, no. 2, p. 988, 2022. [Online]. Available: https://www.mdpi.com/1422-0067/23/2/988.
[56] M. Gozutok, V. Sadhu, and H. T. Sasmazel, "Development of poly (vinyl alcohol)(PVA)/reduced graphene oxide (rGO) electrospun mats," *Journal of Nanoscience and Nanotechnology,* vol. 19, no. 7, pp. 4292-4298, 2019.
[57] Y. Zhong, X. Xia, F. Shi, J. Zhan, J. Tu, and H. J. Fan, "Transition metal carbides and nitrides in energy storage and conversion," *Advanced science,* vol. 3, no. 5, p. 1500286, 2016.
[58] M. Naguib, M. W. Barsoum, and Y. Gogotsi, "Ten years of progress in the synthesis and development of MXenes," *Advanced Materials,* vol. 33, no. 39, p. 2103393, 2021.
[59] I. A. Vasyukova, O. V. Zakharova, D. V. Kuznetsov, and A. A. Gusev, "Synthesis, toxicity assessment, environmental and biomedical applications of MXenes: A review," *Nanomaterials,* vol. 12, no. 11, p. 1797, 2022.
[60] A. Feng, T. Hou, Z. Jia, Y. Zhang, F. Zhang, and G. Wu, "Preparation and characterization of epoxy resin filled with Ti3C2Tx MXene nanosheets with excellent electric conductivity," *Nanomaterials,* vol. 10, no. 1, p. 162, 2020.
[61] L. Liu *et al.*, "Exfoliation and delamination of Ti3C2T x MXene prepared via molten salt etching route," *ACS nano,* vol. 16, no. 1, pp. 111-118, 2021.
[62] Y. Guan *et al.*, "A hydrofluoric acid-free synthesis of 2D vanadium carbide (V2C) MXene for supercapacitor electrodes," *2D Materials,* vol. 7, no. 2, p. 025010, 2020.
[63] N. Driscoll *et al.*, "Two-dimensional Ti3C2 MXene for high-resolution neural interfaces," *Acs Nano,* vol. 12, no. 10, pp. 10419-10429, 2018.
[64] F. Ming, H. Liang, G. Huang, Z. Bayhan, and H. N. Alshareef, "MXenes for rechargeable batteries beyond the lithium-ion," *Advanced Materials,* vol. 33, no. 1, p. 2004039, 2021.
[65] P. Urbankowski *et al.*, "Synthesis of two-dimensional titanium nitride Ti 4 N 3 (MXene)," *Nanoscale,* vol. 8, no. 22, pp. 11385-11391, 2016.
[66] M. Li *et al.*, "Element replacement approach by reaction with Lewis acidic molten salts to synthesize nanolaminated MAX phases and MXenes," *Journal of the American Chemical Society,* vol. 141, no. 11, pp. 4730-4737, 2019.
[67] W. Sun *et al.*, "Electrochemical etching of Ti 2 AlC to Ti 2 CT x (MXene) in low-concentration hydrochloric acid solution," *Journal of Materials Chemistry A,* vol. 5, no. 41, pp. 21663-21668, 2017.
[68] S. Yang *et al.*, "Fluoride-free synthesis of two-dimensional titanium carbide (MXene) using a binary aqueous system," *Angewandte Chemie,* vol. 130, no. 47, pp. 15717-15721, 2018.
[69] J.-C. Lei, X. Zhang, and Z. Zhou, "Recent advances in MXene: Preparation, properties, and applications," *Frontiers of Physics,* vol. 10, pp. 276-286, 2015.
[70] X. Zhan, C. Si, J. Zhou, and Z. Sun, "MXene and MXene-based composites: synthesis, properties and environment-related applications," *Nanoscale Horizons,* vol. 5, no. 2, pp. 235-258, 2020.
[71] S. Jung, U. Zafar, L. S. K. Achary, and C. M. Koo, "Ligand chemistry for surface functionalization in MXenes: A review," *EcoMat,* vol. 5, no. 10, p. e12395, 2023.

View Article Online
DOI: 10.1039/D4NH00209A



[72] R. Ibragimova, P. Erhart, P. Rinke, and H.-P. Komsa, "Surface Functionalization of 2D MXenes: Trends in Distribution, Composition, and Electronic Properties," *The Journal of Physical Chemistry Letters,* vol. 12, no. 9, pp. 2377-2384, 2021/03/11 2021, doi: 10.1021/acs.jpclett.0c03710.

[73] H. Lin, Y. Chen, and J. Shi, "Insights into 2D MXenes for versatile biomedical applications: current advances and challenges ahead," *Advanced Science,* vol. 5, no. 10, p. 1800518, 2018.

[74] R. Li, L. Zhang, L. Shi, and P. Wang, "MXene Ti3C2: An Effective 2D Light-to-Heat Conversion Material," *ACS Nano,* vol. 11, no. 4, pp. 3752-3759, 2017/04/25 2017, doi: 10.1021/acsnano.6b08415.

[75] W. Gao *et al.*, "3D CNT/MXene microspheres for combined photothermal/photodynamic/chemo for cancer treatment," *Frontiers in Bioengineering and Biotechnology,* vol. 10, 2022.

[76] J. Chen *et al.*, "Advances in nanomaterials for photodynamic therapy applications: Status and challenges," *Biomaterials,* vol. 237, p. 119827, 2020.

[77] G. Liu *et al.*, "Surface modified Ti3C2 MXene nanosheets for tumor targeting photothermal/photodynamic/chemo synergistic therapy," *ACS applied materials & interfaces,* vol. 9, no. 46, pp. 40077-40086, 2017.

[78] X. Yu, X. Cai, H. Cui, S.-W. Lee, X.-F. Yu, and B. Liu, "Fluorine-free preparation of titanium carbide MXene quantum dots with high near-infrared photothermal performances for cancer therapy," *Nanoscale,* 10.1039/C7NR05997C vol. 9, no. 45, pp. 17859-17864, 2017, doi: 10.1039/C7NR05997C.

[79] A. Szuplewska *et al.*, "2D Ti2C (MXene) as a novel highly efficient and selective agent for photothermal therapy," *Materials Science and Engineering: C,* vol. 98, pp. 874-886, 2019.

[80] Y. Liu *et al.*, "Two-dimensional MXene/cobalt nanowire heterojunction for controlled drug delivery and chemo-photothermal therapy," *Materials Science and Engineering: C,* vol. 116, p. 111212, 2020/11/01/ 2020, doi: https://doi.org/10.1016/j.msec.2020.111212.

[81] Y. Xu *et al.*, "2D-ultrathin MXene/DOXjade platform for iron chelation chemo-photothermal therapy," *Bioactive Materials,* vol. 14, pp. 76-85, 2022.

[82] E. A. Hussein *et al.*, "Plasmonic MXene-based nanocomposites exhibiting photothermal therapeutic effects with lower acute toxicity than pure MXene," *International Journal of Nanomedicine,* vol. 14, pp. 4529-4539, 2019/12/31 2019, doi: 10.2147/IJN.S202208.

[83] Y. Li *et al.*, "Muscle-inspired MXene/PVA hydrogel with high toughness and photothermal therapy for promoting bacteria-infected wound healing," *Biomaterials Science,* 10.1039/D1BM01604K vol. 10, no. 4, pp. 1068-1082, 2022, doi: 10.1039/D1BM01604K.

[84] F. Li *et al.*, "A bifunctional MXene-modified scaffold for photothermal therapy and maxillofacial tissue regeneration," *Regenerative Biomaterials,* vol. 8, no. 6, p. rbab057, 2021, doi: 10.1093/rb/rbab057.

[85] L. Yang *et al.*, "Low-Temperature Photothermal Therapy Based on Borneol-Containing Polymer-Modified MXene Nanosheets," *ACS Applied Materials & Interfaces,* vol. 14, no. 40, pp. 45178-45188, 2022/10/12 2022, doi: 10.1021/acsami.2c12839.

[86] Y. Ding *et al.*, "Mxene composite fibers with advanced thermal management for inhibiting tumor recurrence and accelerating wound healing," *Chemical Engineering Journal,* vol. 459, p. 141529, 2023.

[87] A. Arabi Shamsabadi, M. Sharifian Gh, B. Anasori, and M. Soroush, "Antimicrobial mode-of-action of colloidal Ti3C2T x MXene nanosheets," *ACS sustainable chemistry & engineering,* vol. 6, no. 12, pp. 16586-16596, 2018.

[88] X. Zhu *et al.*, "A near-infrared light-mediated antimicrobial based on Ag/Ti 3 C 2 T x for effective synergetic antibacterial applications," *Nanoscale,* vol. 12, no. 37, pp. 19129-19141, 2020.

View Article Online
DOI: 10.1039/D4NH00209A

[89] P. Zhang, X.-J. Yang, P. Li, Y. Zhao, and Q. J. Niu, "Fabrication of novel MXene (Ti 3 C 2)/polyacrylamide nanocomposite hydrogels with enhanced mechanical and drug release properties," *Soft Matter,* vol. 16, no. 1, pp. 162-169, 2020.

[90] X. Yang, C. Zhang, D. Deng, Y. Gu, H. Wang, and Q. Zhong, "Multiple stimuli-responsive MXene-based hydrogel as intelligent drug delivery carriers for deep chronic wound healing," *Small,* vol. 18, no. 5, p. 2104368, 2022.

[91] R. Maleki and A. Alamdari, "Tuning the surface chemistry of 2D MXenes for optimizing the micellization of bio-targeted carriers," *Physica E: Low-dimensional Systems and Nanostructures,* vol. 144, p. 115461, 2022/10/01/ 2022, doi: https://doi.org/10.1016/j.physe.2022.115461.

[92] H. Lin, X. Wang, L. Yu, Y. Chen, and J. Shi, "Two-dimensional ultrathin MXene ceramic nanosheets for photothermal conversion," *Nano letters,* vol. 17, no. 1, pp. 384-391, 2017.

[93] H. Wen, P. Liu, Z. Jiang, H. Peng, and H. Liu, "Redox-responsive MXene-SS-PEG nanomaterials for delivery of doxorubicin," *Inorganic Chemistry Communications,* vol. 147, p. 110227, 2023/01/01/ 2023, doi: https://doi.org/10.1016/j.inoche.2022.110227.

[94] Z. Wu, J. Shi, P. Song, J. Li, and S. Cao, "Chitosan/hyaluronic acid based hollow microcapsules equipped with MXene/gold nanorods for synergistically enhanced near infrared responsive drug delivery," *International Journal of Biological Macromolecules,* vol. 183, pp. 870-879, 2021/07/31/ 2021, doi: https://doi.org/10.1016/j.ijbiomac.2021.04.164.

[95] Y. Dong, S. Li, X. Li, and X. Wang, "Smart MXene/agarose hydrogel with photothermal property for controlled drug release," *International Journal of Biological Macromolecules,* vol. 190, pp. 693-699, 2021/11/01/ 2021, doi: https://doi.org/10.1016/j.ijbiomac.2021.09.037.

[96] B. Zhu, J. Shi, C. Liu, J. Li, and S. Cao, "In-situ self-assembly of sandwich-like Ti3C2 MXene/gold nanorods nanosheets for synergistically enhanced near-infrared responsive drug delivery," *Ceramics International,* vol. 47, no. 17, pp. 24252-24261, 2021/09/01/ 2021, doi: https://doi.org/10.1016/j.ceramint.2021.05.136.

[97] A. Liu *et al.*, "Engineering of surface modified Ti3C2Tx MXene based dually controlled drug release system for synergistic multitherapies of cancer," *Chemical Engineering Journal,* vol. 448, p. 137691, 2022/11/15/ 2022, doi: https://doi.org/10.1016/j.cej.2022.137691.

[98] L. Jin *et al.*, "NIR-responsive MXene nanobelts for wound healing," *NPG Asia Materials,* vol. 13, no. 1, p. 24, 2021/03/08 2021, doi: 10.1038/s41427-021-00289-w.

[99] L. Jin *et al.*, "Nanofibers and hydrogel hybrid system with synergistic effect of anti-inflammatory and vascularization for wound healing," *Materials Today Advances,* vol. 14, p. 100224, 2022.

[100] K. Salimiyan rizi, "MXene nanosheets as a novel nanomaterial with antimicrobial applications: A literature review," *Journal of Molecular Structure,* vol. 1262, p. 132958, 2022/08/15/ 2022, doi: https://doi.org/10.1016/j.molstruc.2022.132958.

[101] K. Rasool, M. Helal, A. Ali, C. E. Ren, Y. Gogotsi, and K. A. Mahmoud, "Antibacterial Activity of Ti3C2Tx MXene," *ACS Nano,* vol. 10, no. 3, pp. 3674-3684, 2016/03/22 2016, doi: 10.1021/acsnano.6b00181.

[102] A. Arabi Shamsabadi, M. Sharifian Gh, B. Anasori, and M. Soroush, "Antimicrobial Mode-of-Action of Colloidal Ti3C2Tx MXene Nanosheets," *ACS Sustainable Chemistry & Engineering,* vol. 6, no. 12, pp. 16586-16596, 2018/12/03 2018, doi: 10.1021/acssuschemeng.8b03823.

[103] X. Zhu *et al.*, "A near-infrared light-mediated antimicrobial based on Ag/Ti3C2Tx for effective synergetic antibacterial applications," *Nanoscale,* 10.1039/D0NR04925E vol. 12, no. 37, pp. 19129-19141, 2020, doi: 10.1039/D0NR04925E.

[104] S. Xu *et al.*, "Electroactive and antibacterial wound dressings based on Ti3C2Tx MXene/poly(ε-caprolactone)/gelatin coaxial electrospun nanofibrous membranes," *Nano Research,* vol. 16, no. 7, pp. 9672-9687, 2023/07/01 2023, doi: 10.1007/s12274-023-5527-z.

View Article Online
DOI: 10.1039/D4NH00209A



[105] S. Khademolqorani *et al.*, "Application Scopes of Miniaturized MXene-Functionalized Electrospun Nanofibers-Based Electrochemical Energy Devices," *Small,* p. 2309572, 2023.
[106] Q. Song *et al.*, "Graphene and MXene nanomaterials: toward high-performance electromagnetic wave absorption in gigahertz band range," *Advanced Functional Materials,* vol. 30, no. 31, p. 2000475, 2020.
[107] Y. Zhang, W. Xia, Y. Wu, and P. Zhang, "Prediction of MXene based 2D tunable band gap semiconductors: GW quasiparticle calculations," *Nanoscale,* vol. 11, no. 9, pp. 3993-4000, 2019.
[108] Z. Ling *et al.*, "Flexible and conductive MXene films and nanocomposites with high capacitance," *Proceedings of the National Academy of Sciences,* vol. 111, no. 47, pp. 16676-16681, 2014.
[109] Y. Li *et al.*, "Toward Smart Sensing by MXene," *Small,* p. 2206126, 2022.
[110] C. Jin and Z. Bai, "MXene-based textile sensors for wearable applications," *ACS sensors,* vol. 7, no. 4, pp. 929-950, 2022.
[111] D. Lei *et al.*, "Roles of MXene in pressure sensing: Preparation, composite structure design, and mechanism," *Advanced Materials,* vol. 34, no. 52, p. 2110608, 2022.
[112] R. B. Rakhi, P. Nayak, C. Xia, and H. N. Alshareef, "Novel amperometric glucose biosensor based on MXene nanocomposite," *Scientific Reports,* vol. 6, no. 1, p. 36422, 2016/11/10 2016, doi: 10.1038/srep36422.
[113] Y. Gao *et al.*, "Microchannel-confined MXene based flexible piezoresistive multifunctional micro-force sensor," *Advanced Functional Materials,* vol. 30, no. 11, p. 1909603, 2020.
[114] S. M. S. Rana, M. T. Rahman, M. Salauddin, H. Cho, and J. Y. Park, "An Electrospun PVDF-TRFE/Mxene Nanofibours Mat-Based Self-Powered Motion Sensor," in *2021 IEEE 34th International Conference on Micro Electro Mechanical Systems (MEMS)*, 25-29 Jan. 2021 2021, pp. 30-33, doi: 10.1109/MEMS51782.2021.9375277.
[115] H. Kang *et al.*, "Research Progress on Two-Dimensional Layered MXene/Elastomer Nanocomposites," (in eng), *Polymers (Basel),* vol. 14, no. 19, Sep 29 2022, doi: 10.3390/polym14194094.
[116] G. Basara *et al.*, "Electrically conductive 3D printed Ti(3)C(2)T(x) MXene-PEG composite constructs for cardiac tissue engineering," (in eng), *Acta Biomater,* vol. 139, pp. 179-189, Feb 2022, doi: 10.1016/j.actbio.2020.12.033.
[117] G. Ye *et al.*, "Mussel-inspired conductive Ti(2)C-cryogel promotes functional maturation of cardiomyocytes and enhances repair of myocardial infarction," (in eng), *Theranostics,* vol. 10, no. 5, pp. 2047-2066, 2020, doi: 10.7150/thno.38876.
[118] G. P. Awasthi *et al.*, "Synthesis, characterizations, and biocompatibility evaluation of polycaprolactone–MXene electrospun fibers," *Colloids and Surfaces A: Physicochemical and Engineering Aspects,* vol. 586, p. 124282, 2020.
[119] S. H. Lee *et al.*, "Ternary MXene-loaded PLCL/collagen nanofibrous scaffolds that promote spontaneous osteogenic differentiation," *Nano Convergence,* vol. 9, no. 1, pp. 1-15, 2022.
[120] J. Yan *et al.*, "Bionic MXene based hybrid film design for an ultrasensitive piezoresistive pressure sensor," *Chemical Engineering Journal,* vol. 431, p. 133458, 2022/03/01/ 2022, doi: https://doi.org/10.1016/j.cej.2021.133458.
[121] J. Fan, M. Yuan, L. Wang, Q. Xia, H. Zheng, and A. Zhou, "MXene supported by cotton fabric as electrode layer of triboelectric nanogenerators for flexible sensors," *Nano Energy,* vol. 105, p. 107973, 2023/01/01/ 2023, doi: https://doi.org/10.1016/j.nanoen.2022.107973.
[122] X. Xu, S. Wang, H. Wu, Y. Liu, F. Xu, and J. Zhao, "A multimodal antimicrobial platform based on MXene for treatment of wound infection," *Colloids and Surfaces B: Biointerfaces,* vol. 207, p. 111979, 2021.

View Article Online
DOI: 10.1039/D4NH00209A

[123] S. Zhang *et al.*, "Titanium carbide/zeolite imidazole framework-8/polylactic acid electrospun membrane for near-infrared regulated photothermal/photodynamic therapy of drug-resistant bacterial infections," *Journal of Colloid and Interface Science,* vol. 599, pp. 390-403, 2021.
[124] E. A. Mayerberger, R. M. Street, R. M. McDaniel, M. W. Barsoum, and C. L. Schauer, "Antibacterial properties of electrospun Ti3C2Tz (MXene)/chitosan nanofibers," *RSC Advances,* 10.1039/C8RA06274A vol. 8, no. 62, pp. 35386-35394, 2018, doi: 10.1039/C8RA06274A.
[125] T. Krasian *et al.*, "Low cytotoxicity, antibacterial property, and curcumin delivery performance of toughness-enhanced electrospun composite membranes based on poly(lactic acid) and MAX phase (Ti3AlC2)," *International Journal of Biological Macromolecules,* vol. 262, p. 129967, 2024/03/01/ 2024, doi: https://doi.org/10.1016/j.ijbiomac.2024.129967.
[126] D. Wang, D. Zhang, P. Li, Z. Yang, Q. Mi, and L. Yu, "Electrospinning of Flexible Poly(vinyl alcohol)/MXene Nanofiber-Based Humidity Sensor Self-Powered by Monolayer Molybdenum Diselenide Piezoelectric Nanogenerator," *Nano-Micro Letters,* vol. 13, no. 1, p. 57, 2021/01/16 2021, doi: 10.1007/s40820-020-00580-5.
[127] A. M. Al-Dhahebi, R. Jose, M. Mustapha, and M. S. M. Saheed, "Ultrasensitive aptasensor using electrospun MXene/polyvinylidene fluoride nanofiber composite for Ochratoxin A detection," *Food Chemistry,* vol. 390, p. 133105, 2022.
[128] C. Zhang *et al.*, "Stretchable, flexible, and breathable MXene/dopamine/thermoplastic polyurethane nanofiber membrane with outstanding strain sensing and electromagnetic interference shielding performances," *Materials Today Communications,* vol. 38, p. 107968, 2024.
[129] L.-P. Nan *et al.*, "Ti3C2Tx MXene-Coated Electrospun PCL Conduits for Enhancing Neurite Regeneration and Angiogenesis," *Frontiers in Bioengineering and Biotechnology,* vol. 10, 2022.
[130] S. Kyrylenko *et al.*, "Bio-functionalization of electrospun polymeric nanofibers by Ti 3 C 2 T x MXene," in *2020 IEEE 10th international conference nanomaterials: applications & properties (NAP)*, 2020: IEEE, pp. 02BA10-1-02BA10-5.
[131] K. Diedkova *et al.*, "Polycaprolactone–MXene Nanofibrous Scaffolds for Tissue Engineering," *ACS Applied Materials & Interfaces,* vol. 15, no. 11, pp. 14033-14047, 2023.
[132] H. q. Zhang, D. w. Lan, X. Li, Z. Li, and F. Y. Dai, "Conductive and antibacterial scaffold with rapid crimping property for application prospect in repair of peripheral nerve injury," *Journal of Applied Polymer Science,* vol. 140, no. 5, p. e53426, 2023.
[133] S. Khademolqorani, H. Tavanai, and F. Ajalloueian, "Mechanical properties of silk plain-weft knitted scaffolds for bladder tissue engineering applications," *Polymers for Advanced Technologies,* vol. 32, no. 6, pp. 2367-2377, 2021.
[134] J. Wu, Y. Yu, and G. Su, "Safety assessment of 2D MXenes: in vitro and in vivo," *Nanomaterials,* vol. 12, no. 5, p. 828, 2022.